Correlations between Fukui Indices and Reactivity Descriptors based on the Sanderson's Principle

Jesús Sánchez-Márquez [1].*

[1] Departamento de Química-Física, Facultad de Ciencias, Campus Universitario Río San Pedro, Universidad de Cádiz, 11510 Puerto Real, Cádiz, Spain

*To whom correspondence should be addressed. E-mail: jesus.sanchezmarquez@uca.es

---

SUPPORTING INFORMATION

FIGURES

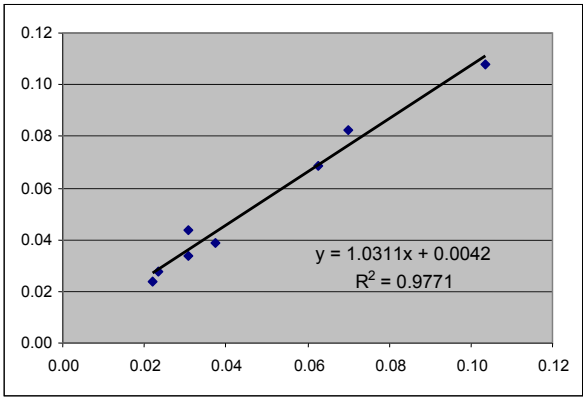

Figure S1. ΔN_A^{max} values calculated with the first model (Eq. 10) vs. ΔN_A^{max} calculated with the second model (Eq. 25) for the molecule CH_2CHCHO. The values of the two parameters have been obtained using the Hirshfeld population analysis.

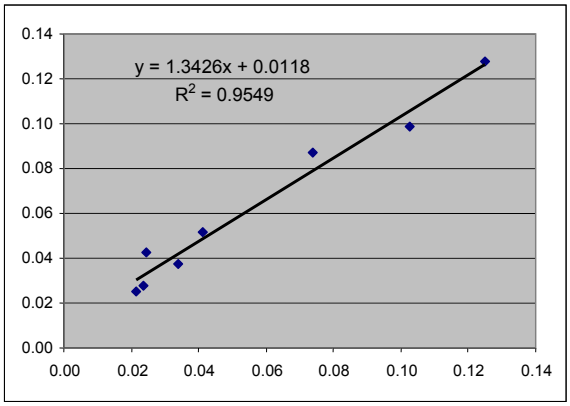

Figure S2. ΔN_A^{max} values calculated with the first model (Eq. 10) vs. ΔN_A^{max} calculated with the second model (Eq. 25) for the molecule CH_2CHNO_2. The values of the two parameters have been obtained using the Hirshfeld population analysis.

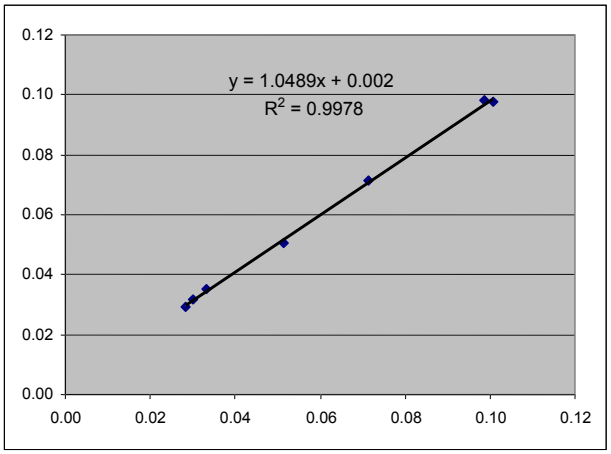

Figure S3. ΔN_A^{max} values calculated with the first model (Eq. 10) vs. ΔN_A^{max} calculated with the second model (Eq. 25) for the molecule CH_2CHCN. The values of the two parameters have been obtained using the Hirshfeld population analysis.

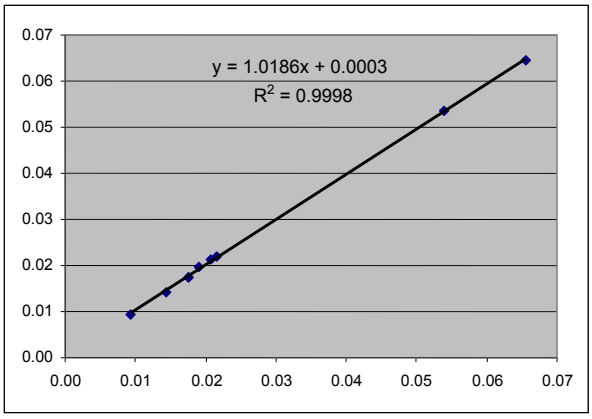

Figure S4. ΔN_A^{max} values calculated with the first model (Eq. 10) vs. ΔN_A^{max} calculated with the second model (Eq. 25) for the molecule CH_2CHCH_3. The values of the two parameters have been obtained using the Hirshfeld population analysis.

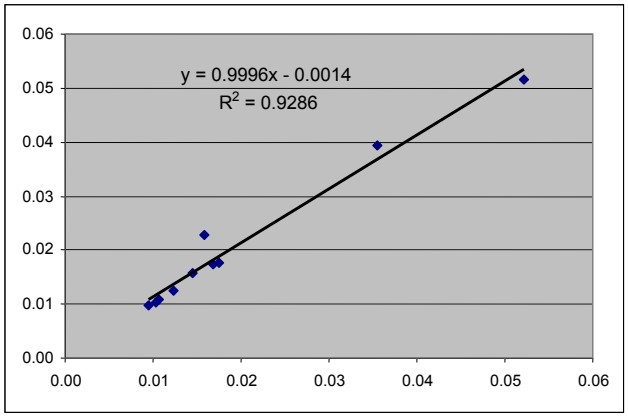

Figure S5. ΔN_A^{max} values calculated with the first model (Eq. 10) vs. ΔN_A^{max} calculated with the second model (Eq. 25) for the molecule CH_2CHOCH_3. The values of the two parameters have been obtained using the Hirshfeld population analysis.

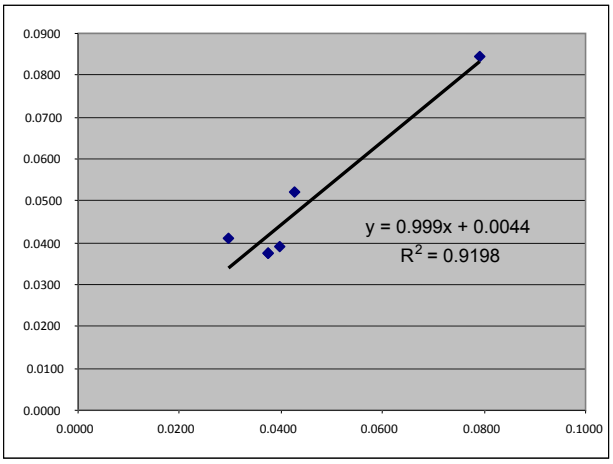

Figure S6. ΔN_A^{max} values calculated with the first model (Eq. 10) vs. ΔN_A^{max} calculated with the second model (Eq. 25) for the molecule CH_2CHCl. The values of the two parameters have been obtained using the population analysis of QTAIM.

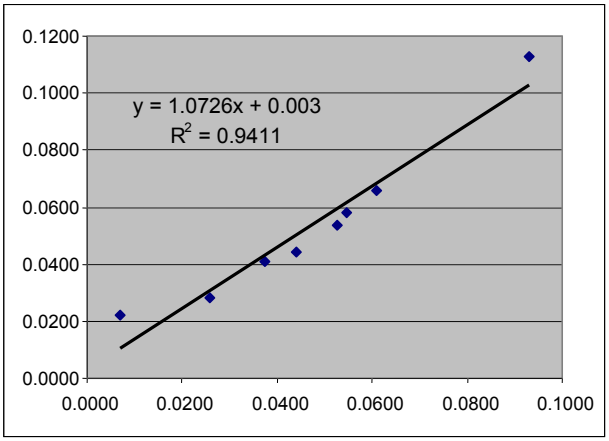

Figure S7. ΔN_A^{max} values calculated with the first model (Eq. 10) vs. ΔN_A^{max} calculated with the second model (Eq. 25) for the molecule CH_2CHCHO. The values of the two parameters have been obtained using the population analysis of QTAIM.

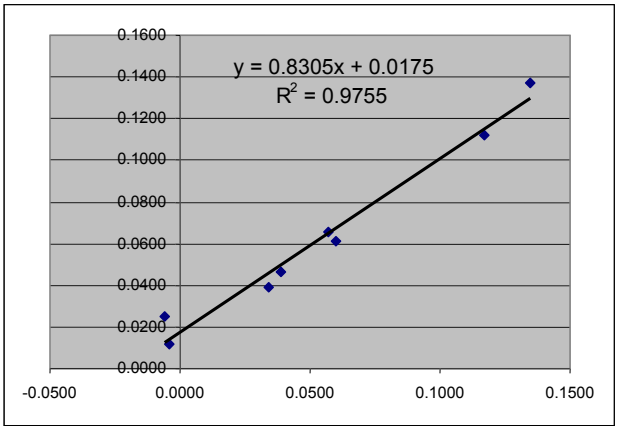

Figure S8. ΔN_A^{max} values calculated with the first model (Eq. 10) vs. ΔN_A^{max} calculated with the second model (Eq. 25) for the molecule CH_2CHNO_2. The values of the two parameters have been obtained using the population analysis of QTAIM.

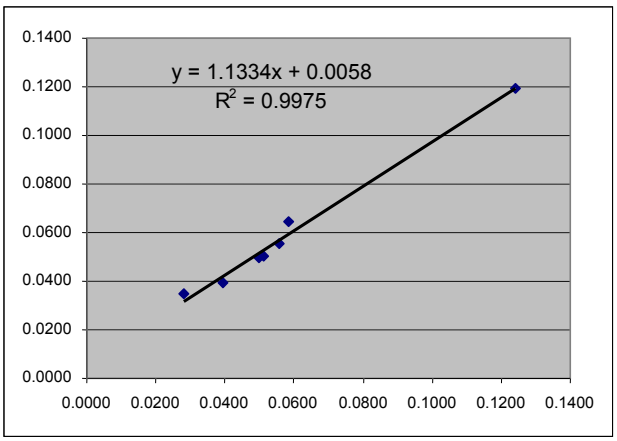

Figure S9. ΔN_A^{max} values calculated with the first model (Eq. 10) vs. ΔN_A^{max} calculated with the second model (Eq. 25) for the molecule CH_2CHCN. The values of the two parameters have been obtained using the population analysis of QTAIM.

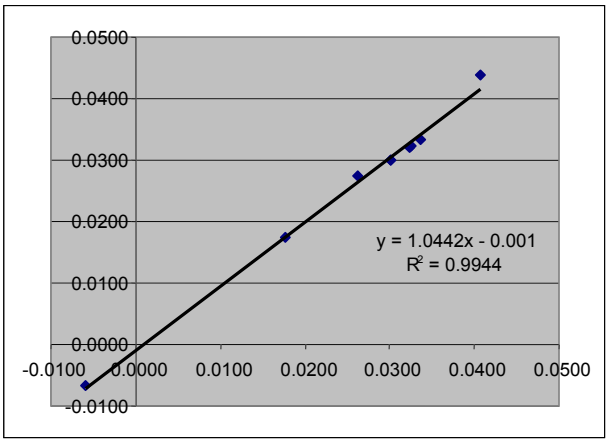

Figure S10. ΔN_A^{max} values calculated with the first model (Eq. 10) vs. ΔN_A^{max} calculated with the second model (Eq. 25) for the molecule CH_2CHCH_3. The values of the two parameters have been obtained using the population analysis of QTAIM.

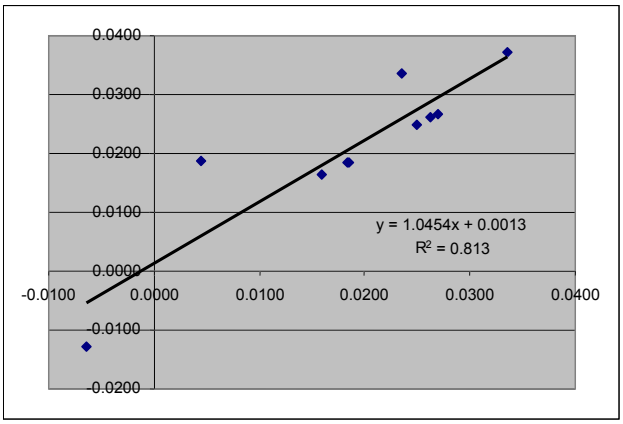

Figure S11. ΔN_A^{max} values calculated with the first model (Eq. 10) vs. ΔN_A^{max} calculated with the second model (Eq. 25) for the molecule CH_2CHOCH_3. The values of the two parameters have been obtained using the population analysis of QTAIM.

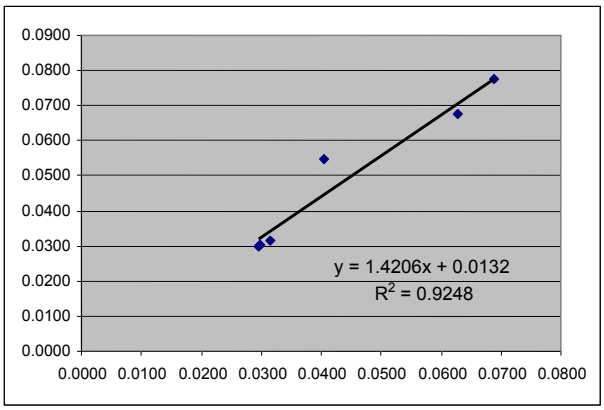

Figure S12. ΔN_A^{max} values calculated with the first model (Eq. 10) vs. ΔN_A^{max} calculated with the second model (Eq. 25) for the molecule CH_2CHCl. The values of the two parameters have been obtained using the Mulliken population analysis.

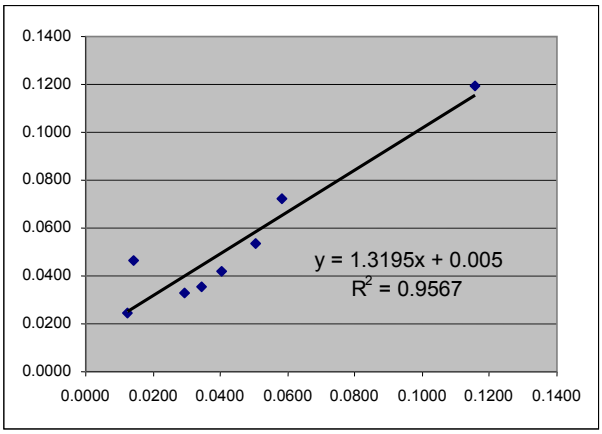

Figure S13. ΔN_A^{max} values calculated with the first model (Eq. 10) vs. ΔN_A^{max} calculated with the second model (Eq. 25) for the molecule CH_2CHCHO. The values of the two parameters have been obtained using the Mulliken population analysis.

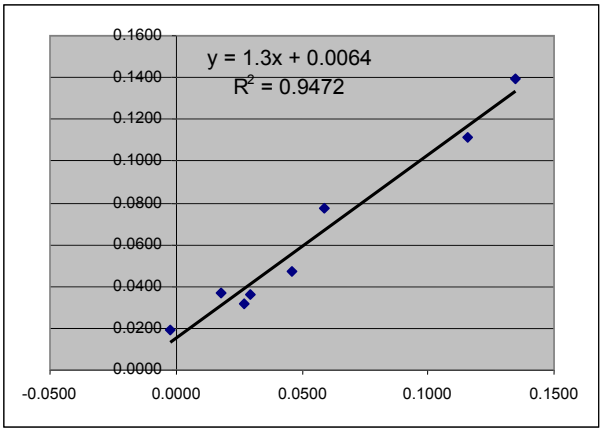

Figure S14. ΔN_A^{max} values calculated with the first model (Eq. 10) vs. ΔN_A^{max} calculated with the second model (Eq. 25) for the molecule CH_2CHNO_2. The values of the two parameters have been obtained using the Mulliken population analysis.

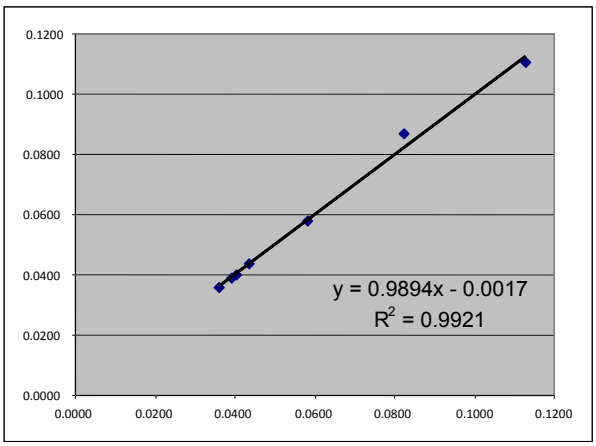

Figure S15. ΔN_A^{max} values calculated with the first model (Eq. 10) vs. ΔN_A^{max} calculated with the second model (Eq. 25) for the molecule CH_2CHCN. The values of the two parameters have been obtained using the Mulliken population analysis.

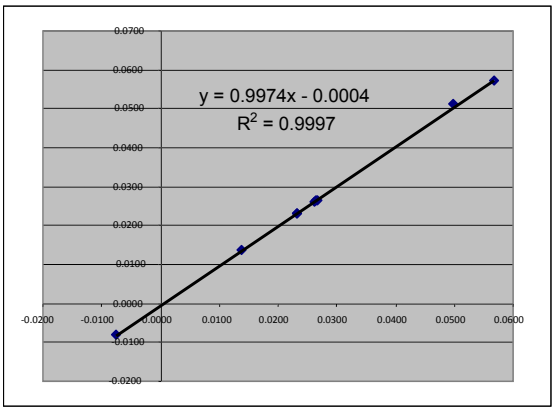

Figure S16. ΔN_A^{max} values calculated with the first model (Eq. 10) vs. ΔN_A^{max} calculated with the second model (Eq. 25) for the molecule CH_2CHCH_3. The values of the two parameters have been obtained using the Mulliken population analysis.

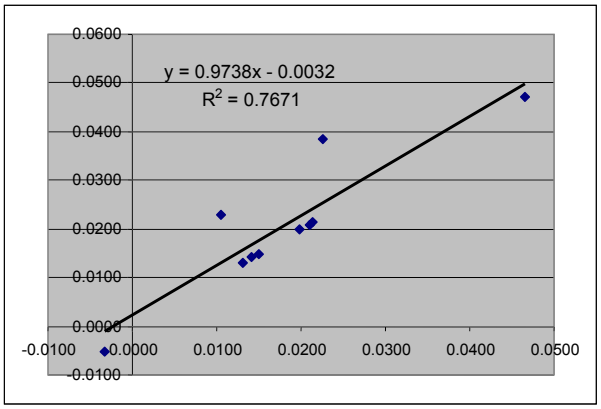

Figure S17. ΔN_A^{max} values calculated with the first model (Eq. 10) vs. ΔN_A^{max} calculated with the second model (Eq. 25) for the molecule CH_2CHOCH_3. The values of the two parameters have been obtained using the Mulliken population analysis.

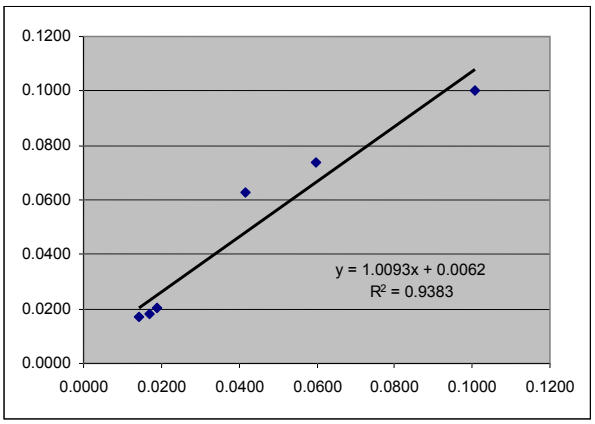

Figure S18. ΔN_A^{max} values calculated with the first model (Eq. 10) vs. ΔN_A^{max} calculated with the second model (Eq. 25) for the molecule CH_2CHCl. The values of the two parameters have been obtained using the Natural Population Analysis.

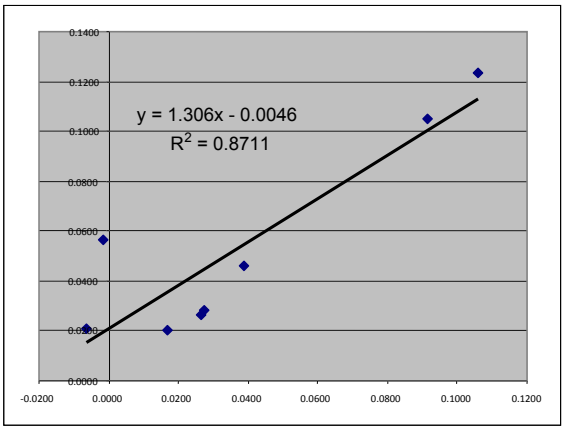

Figure S19. ΔN_A^{max} values calculated with the first model (Eq. 10) vs. ΔN_A^{max} calculated with the second model (Eq. 25) for the molecule CH_2CHCHO. The values of the two parameters have been obtained using the Natural Population Analysis.

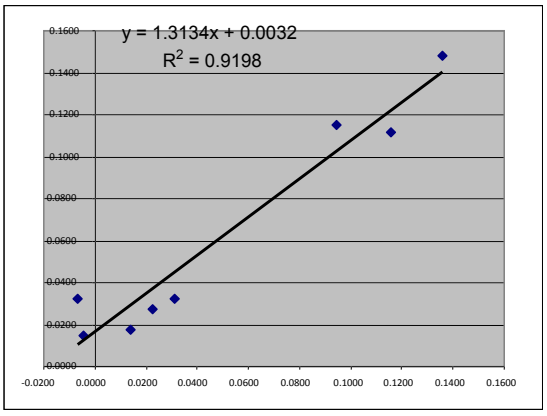

Figure S20. ΔN_A^{max} values calculated with the first model (Eq. 10) vs. ΔN_A^{max} calculated with the second model (Eq. 25) for the molecule CH_2CHNO_2. The values of the two parameters have been obtained using the Natural Population Analysis.

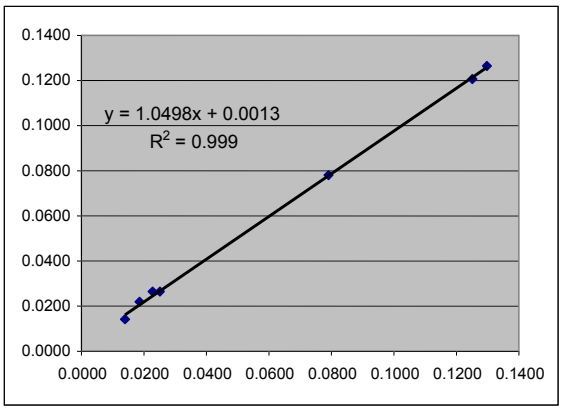

Figure S21. ΔN_A^{max} values calculated with the first model (Eq. 10) vs. ΔN_A^{max} calculated with the second model (Eq. 25) for the molecule CH_2CHCN. The values of the two parameters have been obtained using the Natural Population Analysis.

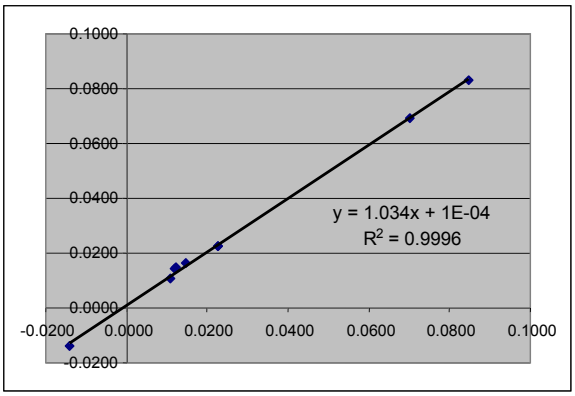

Figure S22. ΔN_A^{max} values calculated with the first model (Eq. 10) vs. ΔN_A^{max} calculated with the second model (Eq. 25) for the molecule CH_2CHCH_3. The values of the two parameters have been obtained using the Natural Population Analysis.

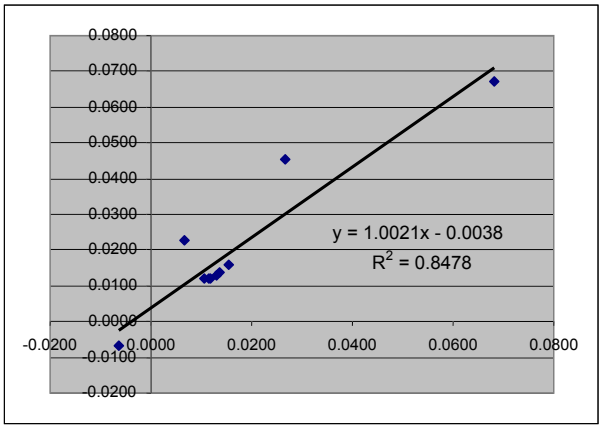

Figure S23. ΔN_A^{max} values calculated with the first model (Eq. 10) vs. ΔN_A^{max} calculated with the second model (Eq. 25) for the molecule CH_2CHOCH_3. The values of the two parameters have been obtained using the Natural Population Analysis.

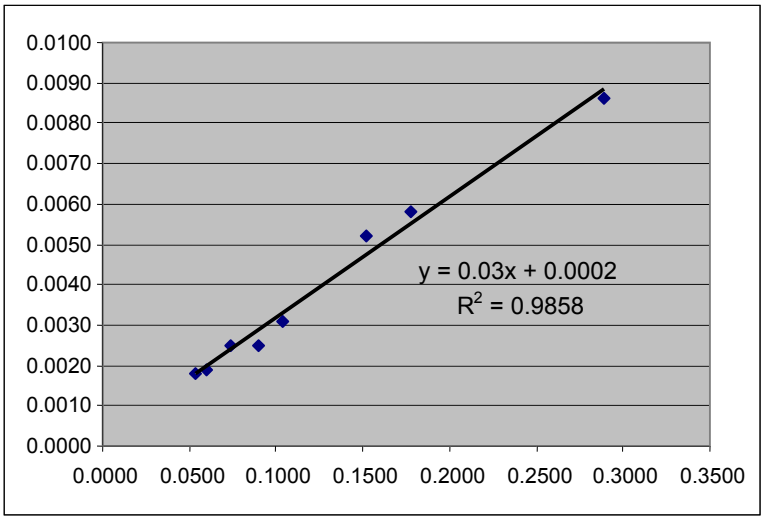

Figure S24. Linear regression ω_A (Eq. 11, first model) versus f_A (Eq. 24, second model) for the molecule CH_2CHCHO. Both parameters have been obtained using the Hirshfeld population analysis.

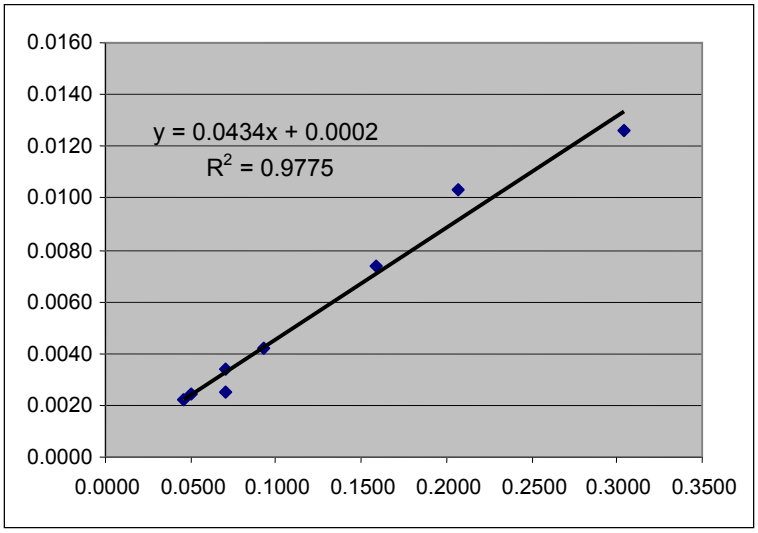

Figure S25. Linear regression ω_A (Eq. 11, first model) versus f_A (Eq. 24, second model) for the molecule CH_2CHNO_2. Both parameters have been obtained using the Hirshfeld population analysis.

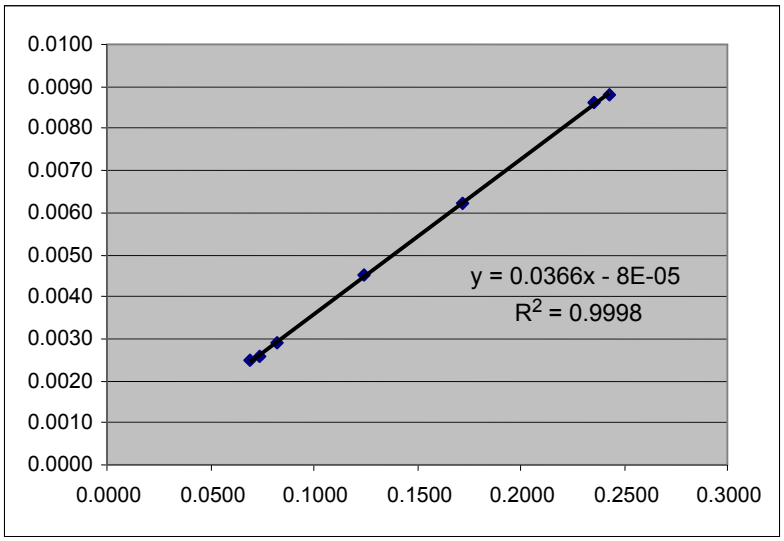

Figure S26. Linear regression ω_A (Eq. 11, first model) versus f_A (Eq. 24, second model) for the molecule CH_2CHCN. Both parameters have been obtained using the Hirshfeld population analysis.

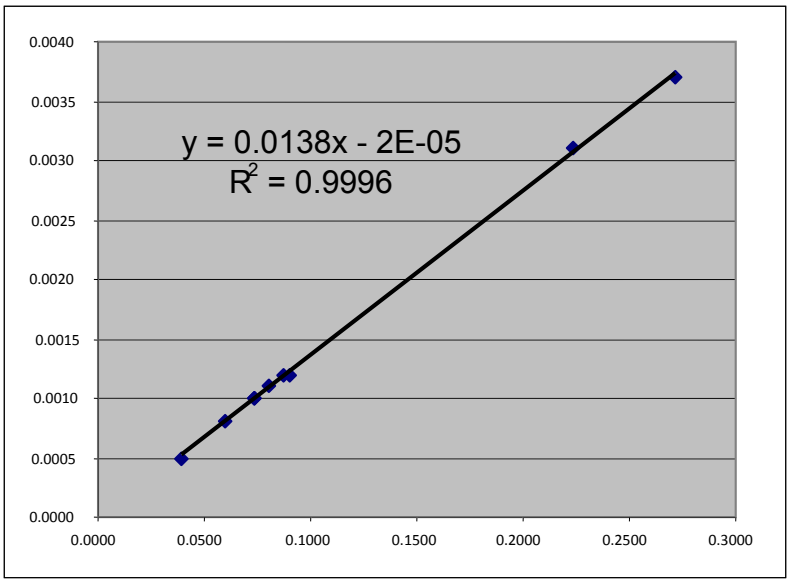

Figure S27. Linear regression ω_A (Eq. 11, first model) versus f_A (Eq. 24, second model) for the molecule CH_2CHCH_3. Both parameters have been obtained using the Hirshfeld population analysis.

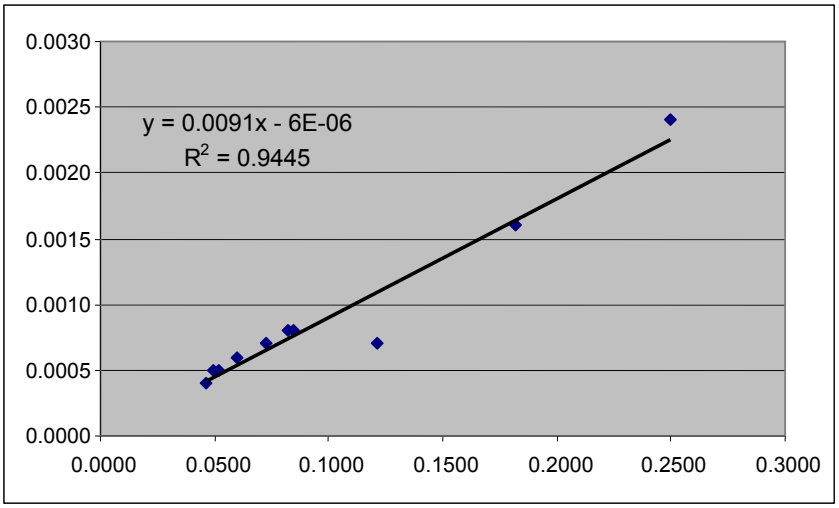

Figure S28. Linear regression ω_A (Eq. 11, first model) versus f_A (Eq. 24, second model) for the molecule CH_2CHOCH_3. Both parameters have been obtained using the Hirshfeld population analysis.

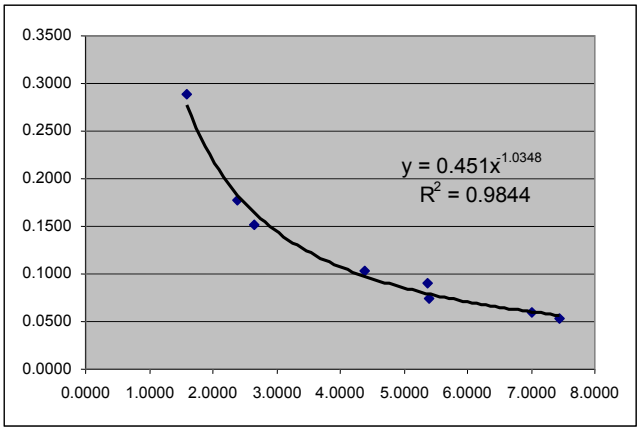

Figure S29. f_A values calculated with the second model (Eq. 24) vs. η_A parameter calculated with the first model (Eq. 8) for the molecule CH_2CHCHO. The values of the two parameters have been obtained using the Hirshfeld population analysis.

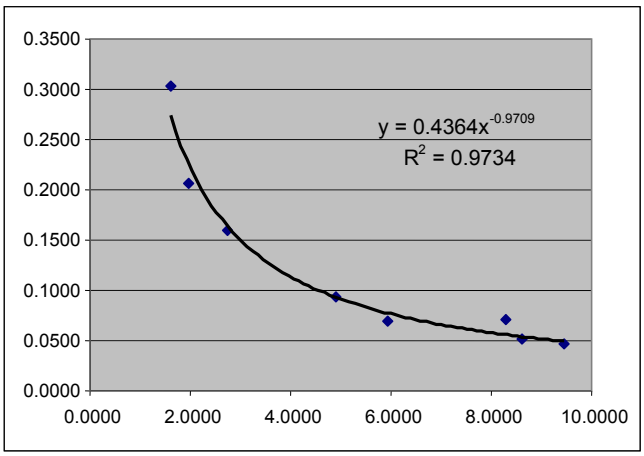

Figure S30. f_A values calculated with the second model (Eq. 24) vs. η_A parameter calculated with the first model (Eq. 8) for the molecule CH_2CHNO_2. The values of the two parameters have been obtained using the Hirshfeld population analysis.

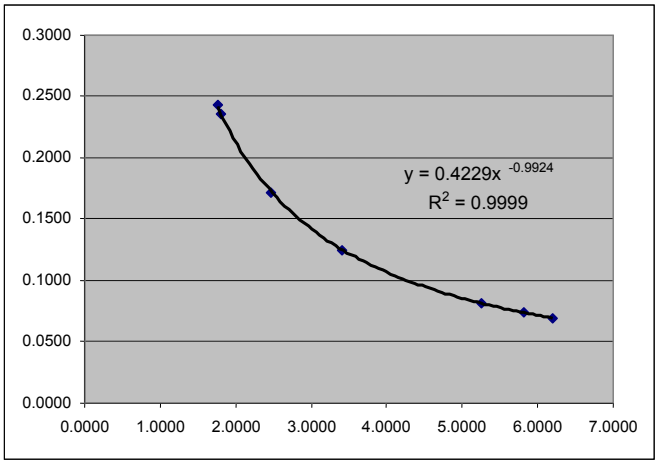

Figure S31. f_A values calculated with the second model (Eq. 24) vs. η_A parameter calculated with the first model (Eq. 8) for the molecule CH_2CHCN. The values of the two parameters have been obtained using the Hirshfeld population analysis.

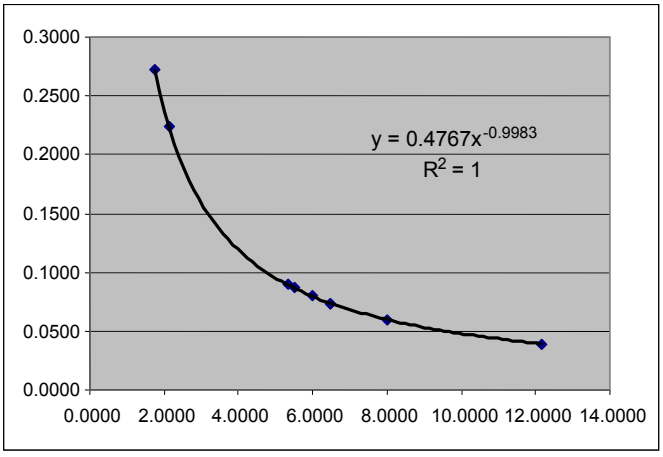

Figure S32. f_A values calculated with the second model (Eq. 24) vs. η_A parameter calculated with the first model (Eq. 8) for the molecule CH_2CHCH_3. The values of the two parameters have been obtained using the Hirshfeld population analysis.

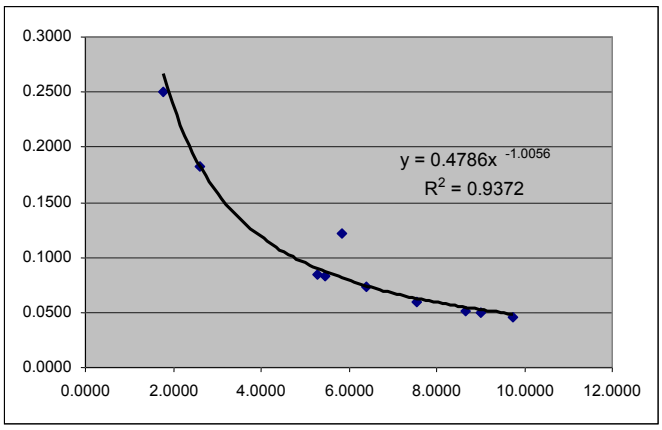

Figure S33. f_A values calculated with the second model (Eq. 24) vs. η_A parameter calculated with the first model (Eq. 8) for the molecule CH_2CHOCH_3. The values of the two parameters have been obtained using the Hirshfeld population analysis.

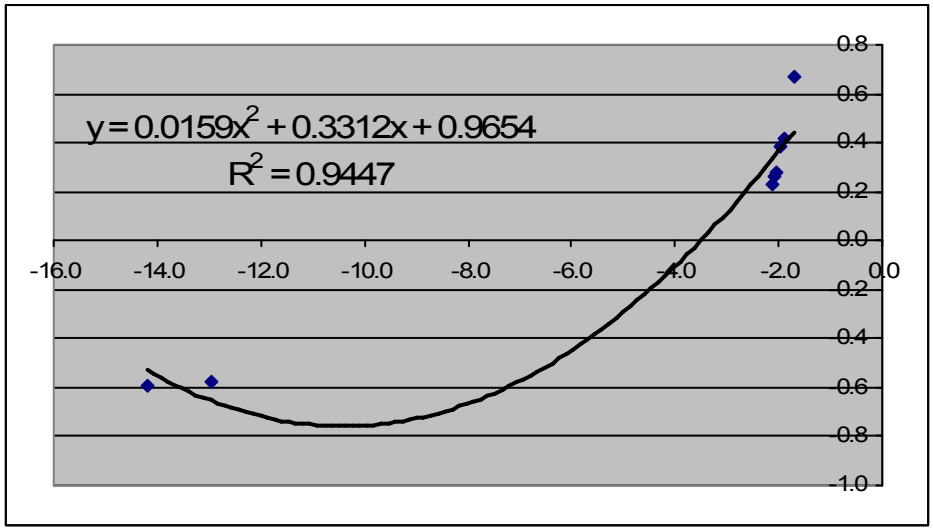

Figure S34. Parabolic regression $\left(f_A^{(2)}/f_A\right)$ versus $1/\Omega_A$ for the molecule CH_2CHCHO. The values of the parameters have been obtained using the Hirshfeld population analysis.

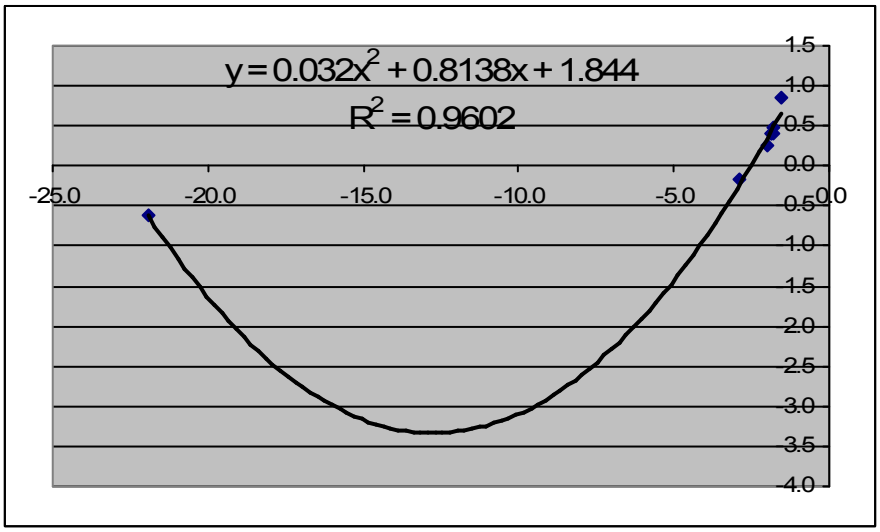

Figure S35. Parabolic regression $\left(f_A^{(2)}/f_A\right)$ versus $1/\Omega_A$ for the molecule CH_2CHNO_2. The values of the parameters have been obtained using the Hirshfeld population analysis.

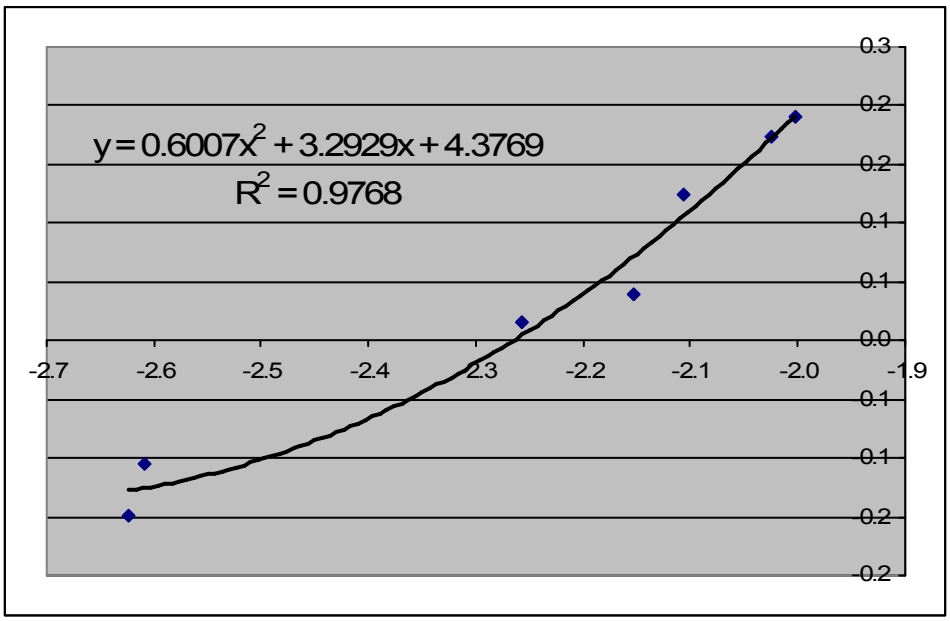

Figure S36. Parabolic regression $\left(f_A^{(2)}/f_A\right)$ versus $1/\Omega_A$ for the molecule CH_2CHCN. The values of the parameters have been obtained using the Hirshfeld population analysis.

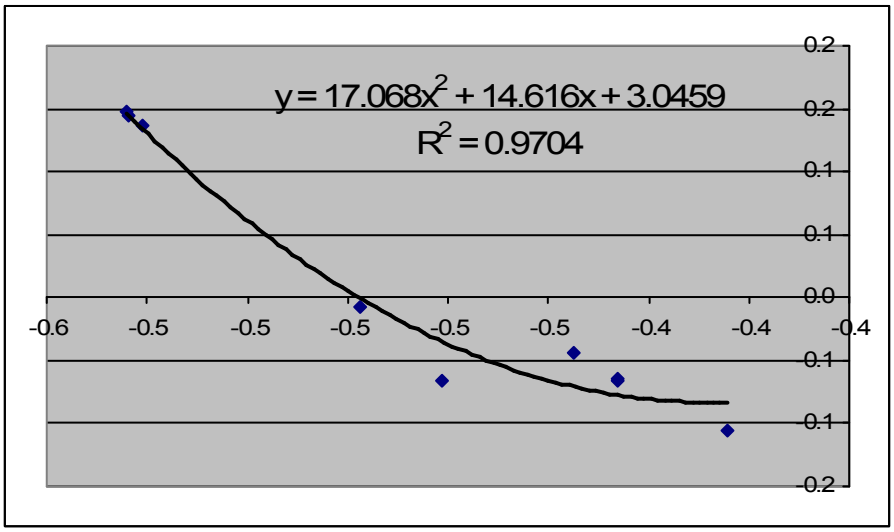

Figure S37. Parabolic regression $\left(f_A^{(2)}/f_A\right)$ versus $1/\Omega_A$ for the molecule CH_2CHCH_3. The values of the parameters have been obtained using the Hirshfeld population analysis.

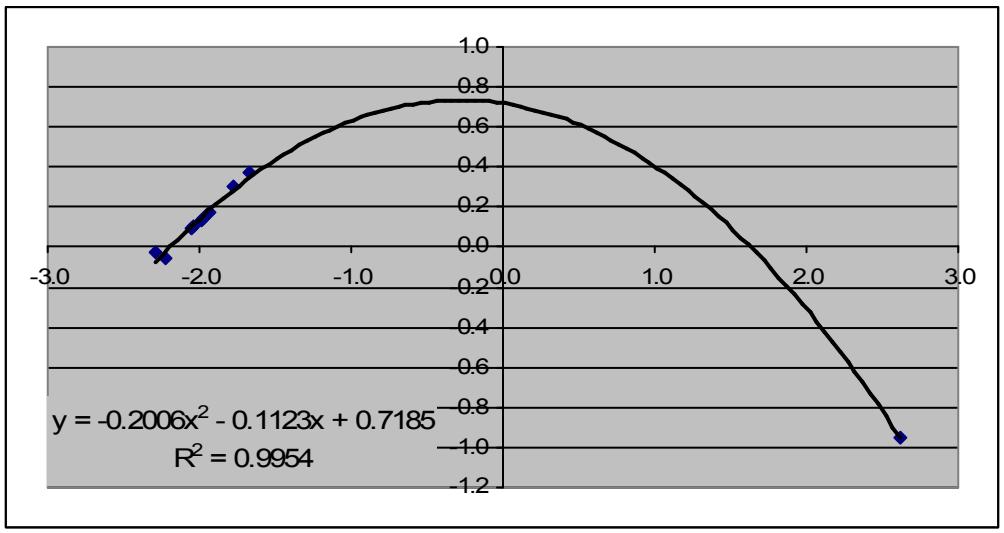

Figure S38. Parabolic regression $\left(f_A^{(2)}/f_A\right)$ versus $1/\Omega_A$ for the molecule CH_2CHOCH_3. The values of the parameters have been obtained using the Hirshfeld population analysis.

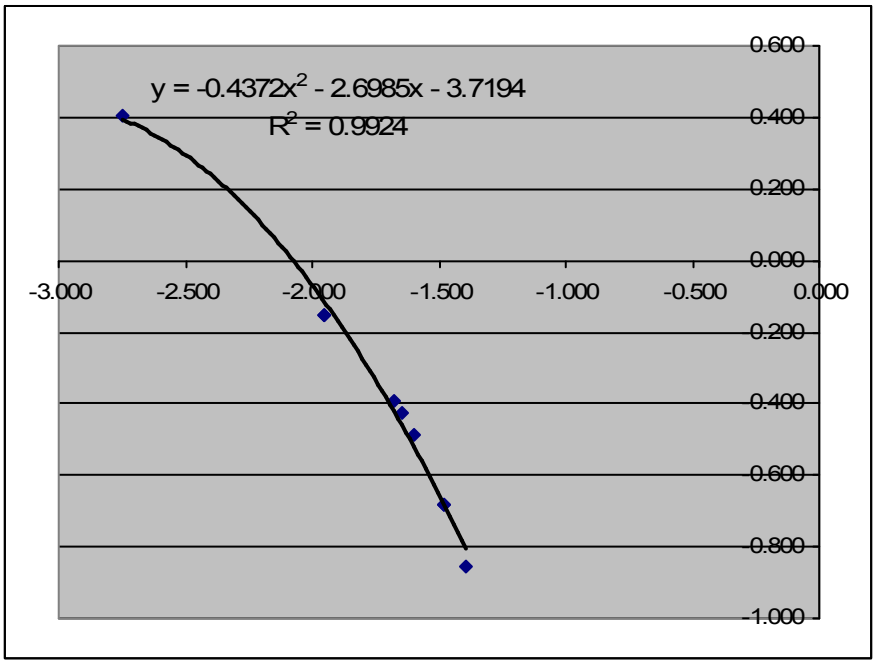

Figure S39. Parabolic regression $\left(f_A^{(2)}/f_A\right)$ versus $1/\Omega_A$ for the molecule CH_3CHSH. The values of the parameters have been obtained using the Hirshfeld population analysis.

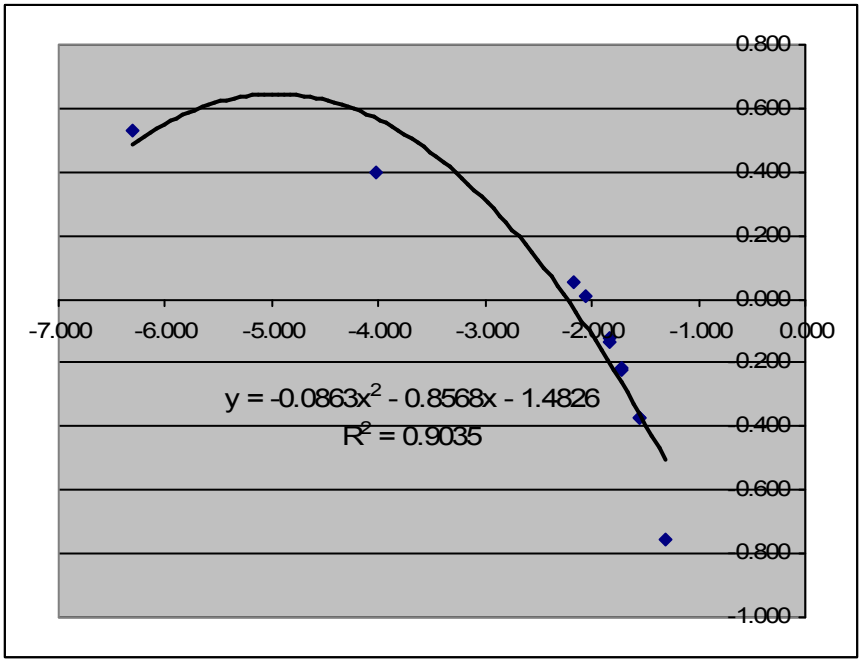

Figure S40. Parabolic regression $\left(f_A^{(2)}/f_A\right)$ versus $1/\Omega_A$ for the molecule CH_3COOCH_3. The values of the parameters have been obtained using the Hirshfeld population analysis.

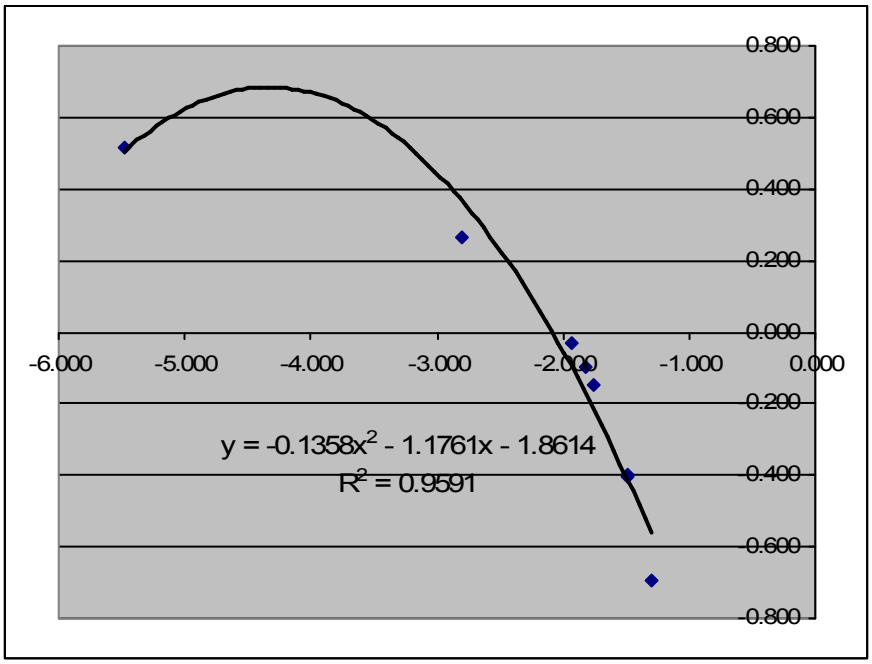

Figure S41. Parabolic regression $\left(f_A^{(2)}/f_A\right)$ versus $1/\Omega_A$ for the molecule CH_3COOH. The values of the parameters have been obtained using the Hirshfeld population analysis.

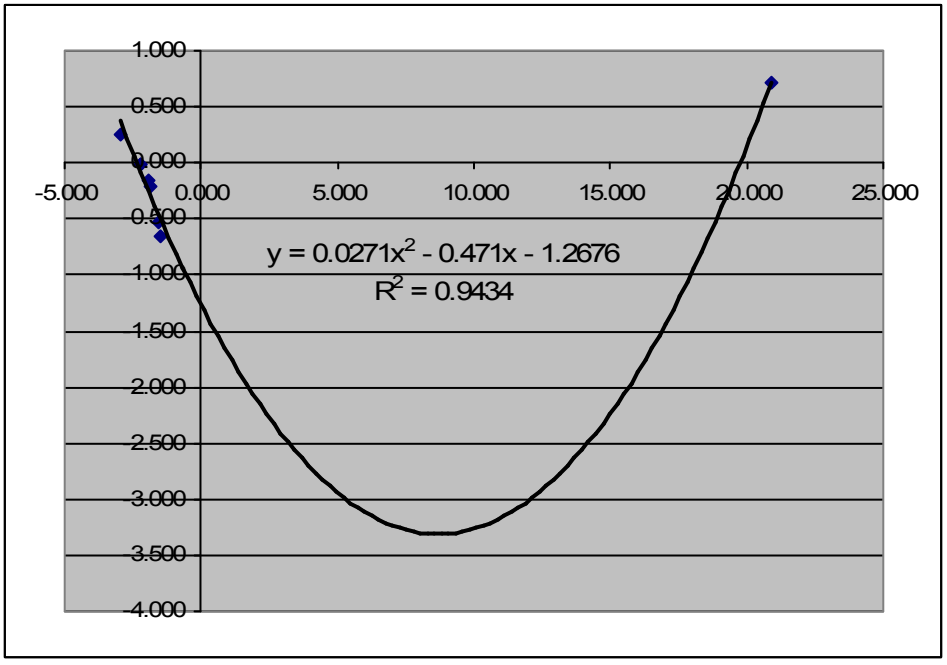

Figure S42. Parabolic regression $\left(f_A^{(2)}/f_A\right)$ versus $1/\Omega_A$ for the molecule CH_2CHNH_2. The values of the parameters have been obtained using the Hirshfeld population analysis.

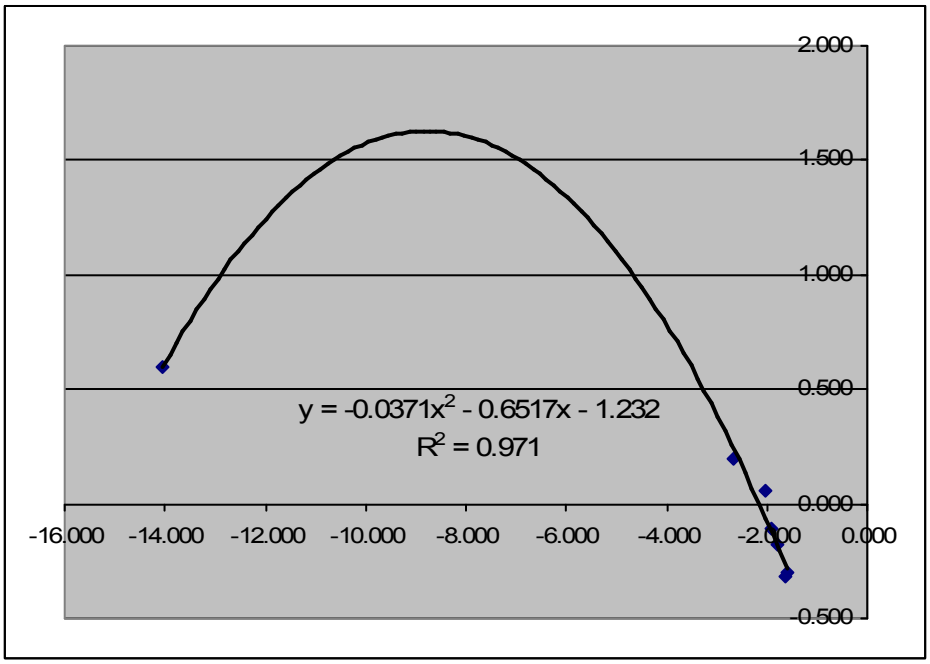

Figure S43. Parabolic regression $\left(f_A^{(2)}/f_A\right)$ versus $1/\Omega_A$ for the molecule CH_2CHOH. The values of the parameters have been obtained using the Hirshfeld population analysis.

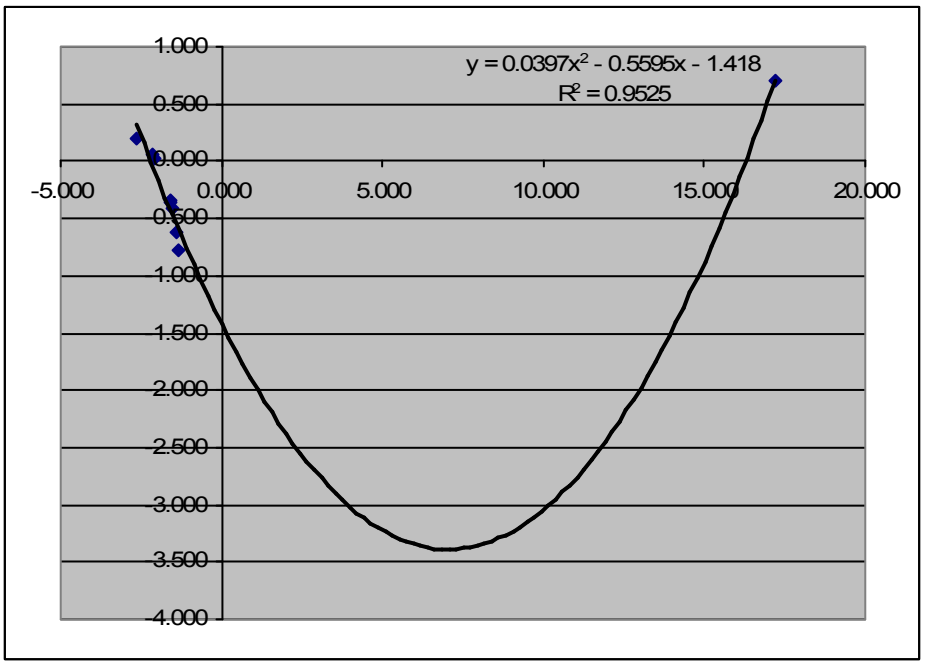

Figure S44. Parabolic regression $\left(f_A^{(2)}/f_A\right)$ versus $1/\Omega_A$ for the molecule CH_3CONH_2. The values of the parameters have been obtained using the Hirshfeld population analysis.

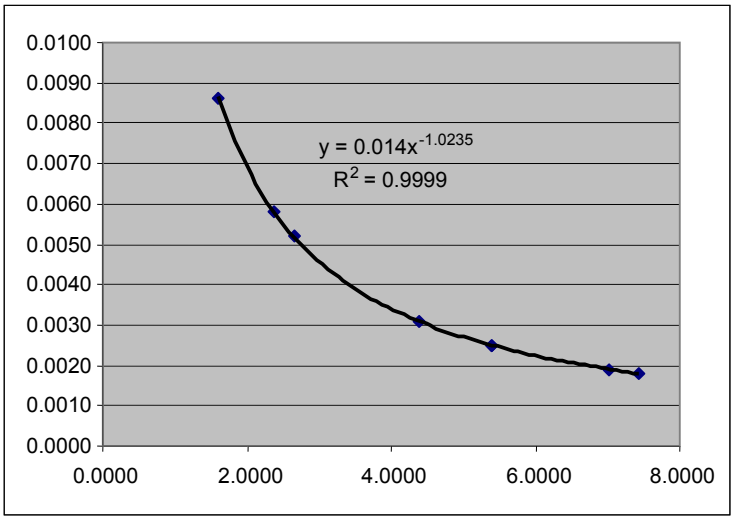

Figure S45. Electrophilicities ω_A versus the local parameter η_A for the CH_2CHCHO molecule. We have used the Hirshfeld population analysis in both cases.

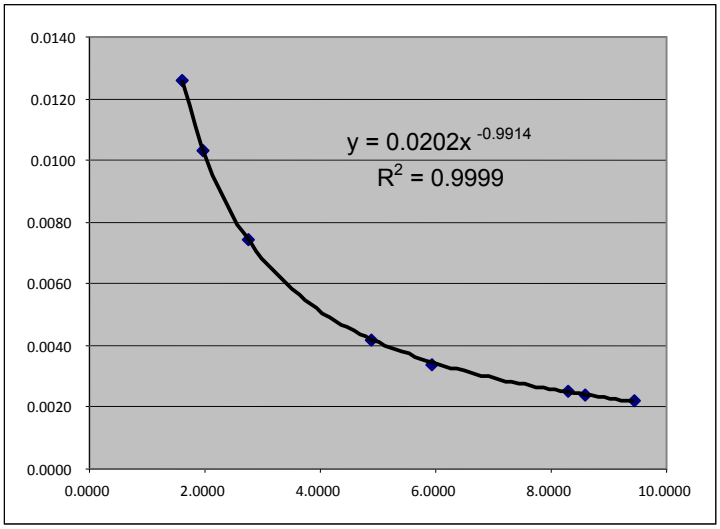

Figure S46. Electrophilicities ω_A versus the local parameter η_A for the CH_2CHNO_2 molecule. We have used the Hirshfeld population analysis in both cases.

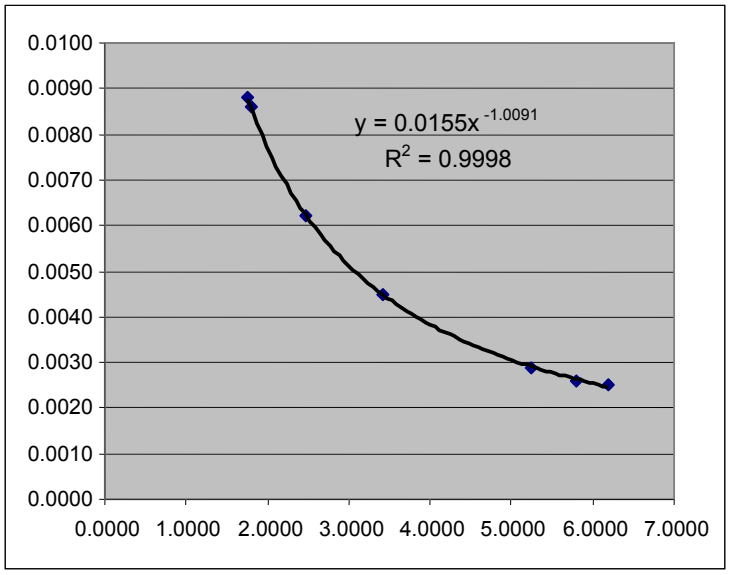

Figure S47. Electrophilicities ω_A versus the local parameter η_A for the CH_2CHCN molecule. We have used the Hirshfeld population analysis in both cases.

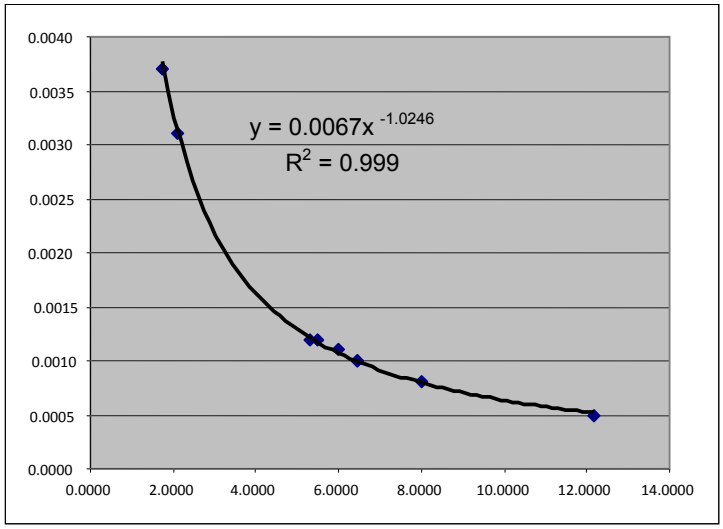

Figure S48. Electrophilicities ω_A versus the local parameter η_A for the CH_2CHCH_3 molecule. We have used the Hirshfeld population analysis in both cases.

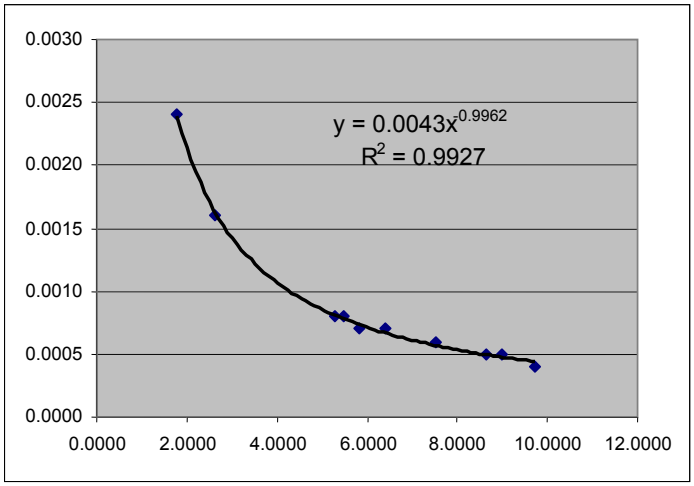

Figure S49. Electrophilicities ω_A versus the local parameter η_A for the CH_2CHOCH_3 molecule. We have used the Hirshfeld population analysis in both cases.

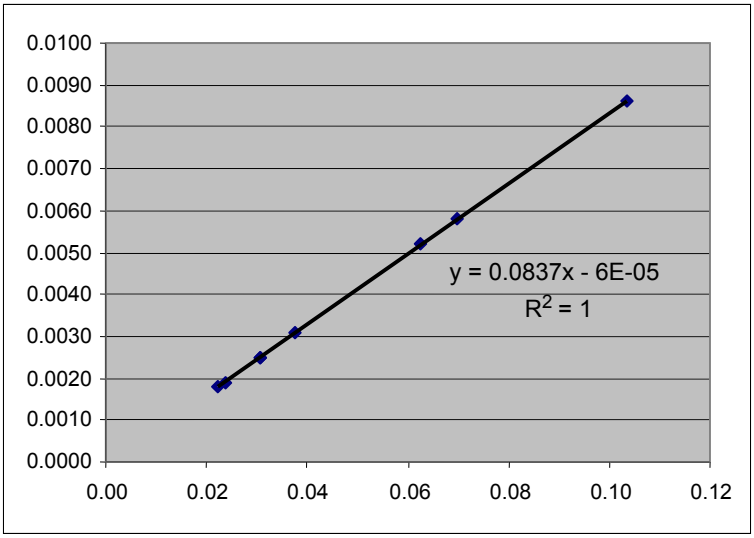

Figure S50. Atomic values ω_A versus local parameter ΔN_A^{max} for the CH_2CHCHO molecule using the Hirshfeld population analysis.

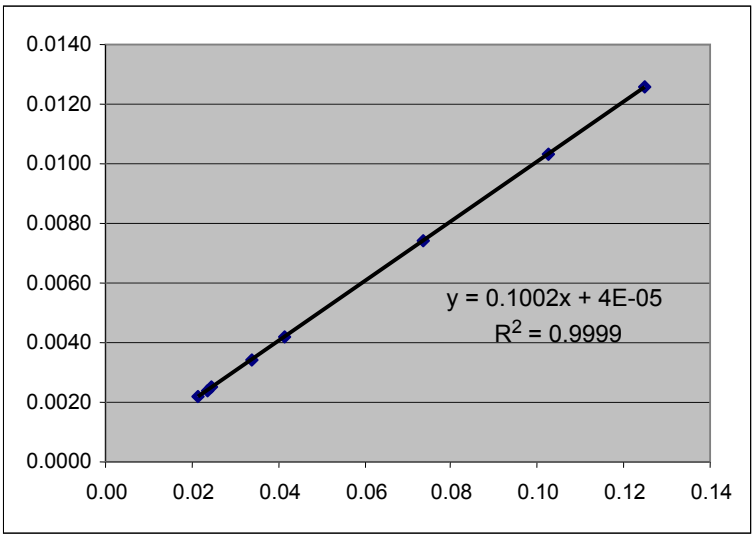

Figure S51. Atomic values ω_A versus local parameter ΔN_A^{max} for the CH_2CHNO_2 molecule using the Hirshfeld population analysis.

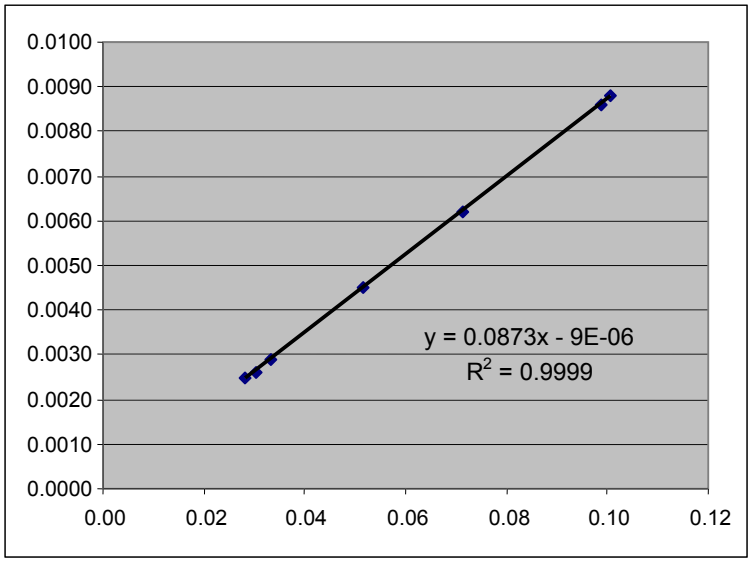

Figure S52. Atomic values ω_A versus local parameter ΔN_A^{max} for the CH_2CHCN molecule using the Hirshfeld population analysis.

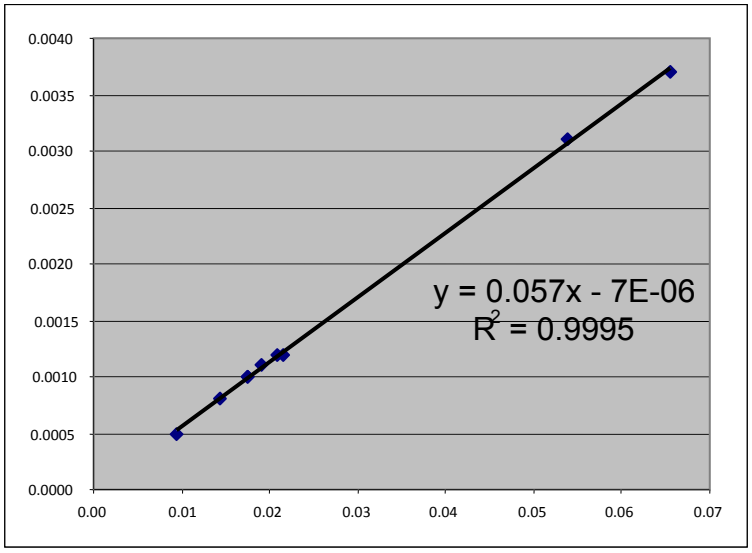

Figure S53. Atomic values ω_A versus local parameter ΔN_A^{max} for the CH_2CHCH_3 molecule using the Hirshfeld population analysis.

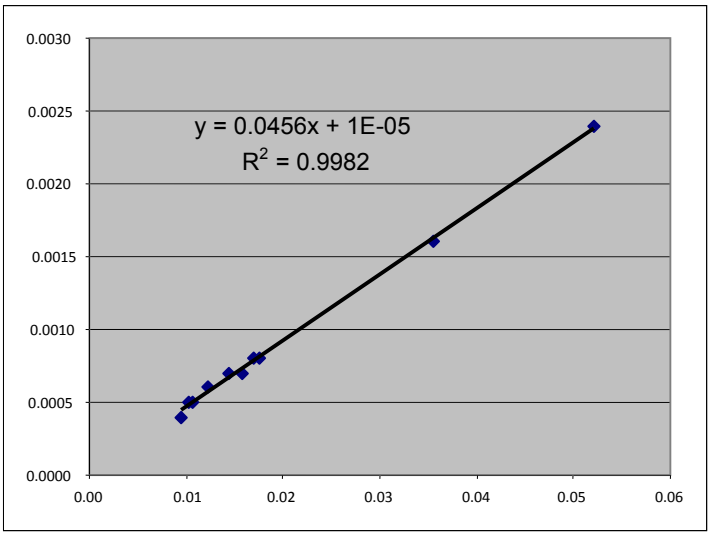

Figure S54. Atomic values ω_A versus local parameter ΔN_A^{max} for the CH_2CHOCH_3 molecule using the Hirshfeld population analysis.

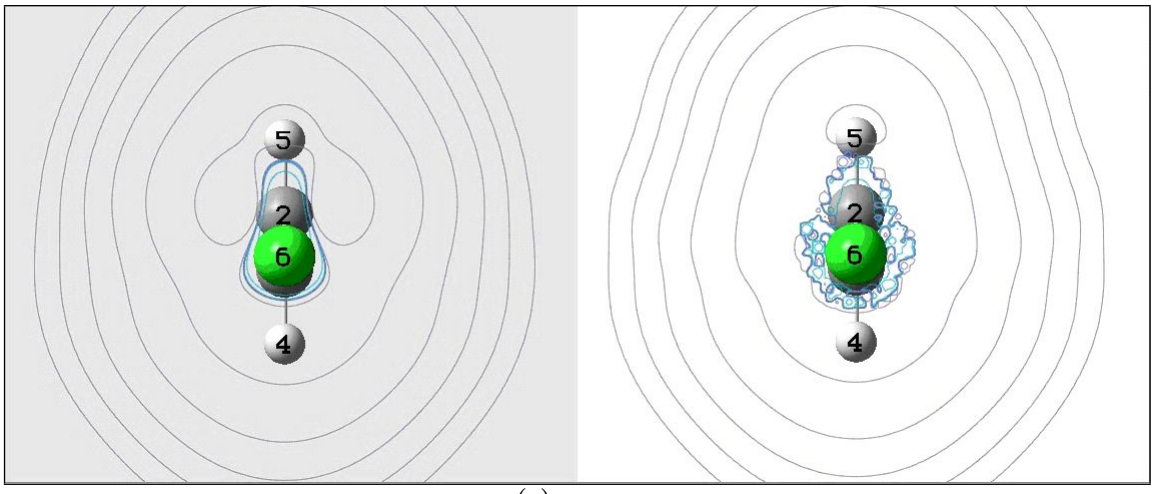

Figure S55. Left) Fukui function $f(\mathbf{r})_{\text{Quadratic expansion}}$ calculated with a parabolic approximation (Eq. 23) and right) hardness function $\eta(\mathbf{r})$ (Eq. 13) for the CH_2CHCl molecule.

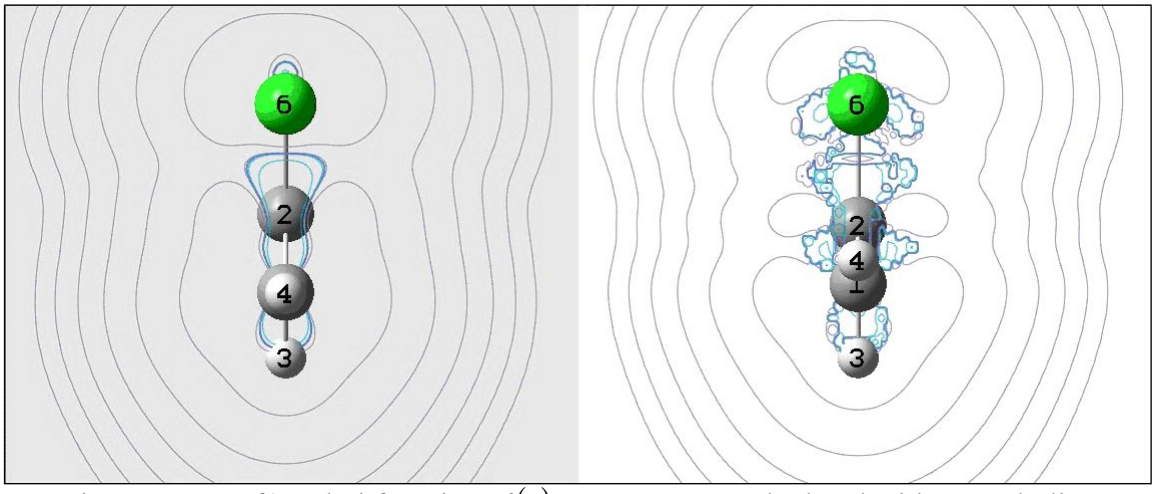

Figure S56. Left) Fukui function $f(\mathbf{r})_{\text{Quadratic expansion}}$ calculated with a parabolic approximation (Eq. 23) and right) hardness function $\eta(\mathbf{r})$ (Eq. 13) for the CH_2CHCl molecule.

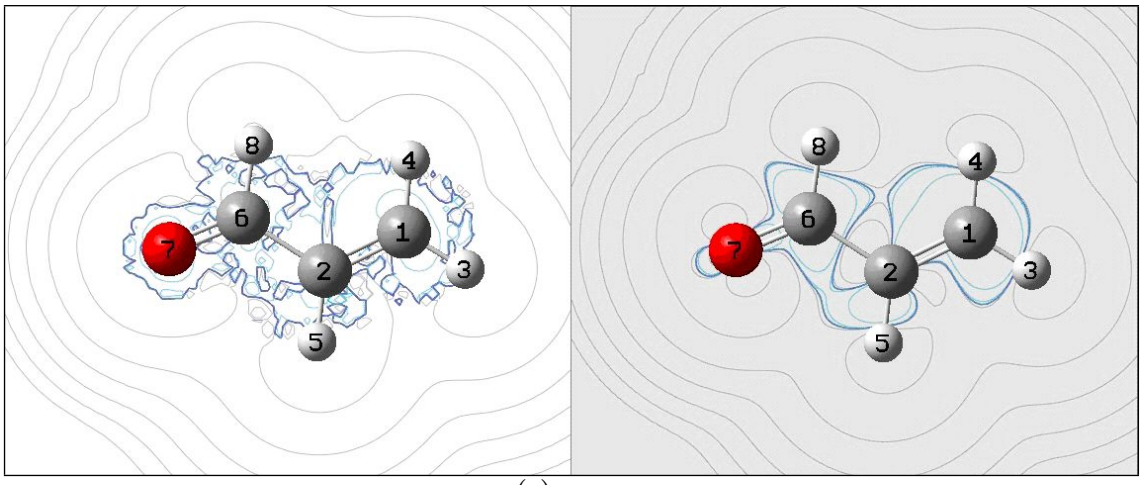

Figure S57. Left) Fukui function $f(\mathbf{r})_{\text{Quadratic expansion}}$ calculated with a parabolic approximation (Eq. 23) and right) hardness function $\eta(\mathbf{r})$ (Eq. 13) for the CH_2CHCHO molecule.

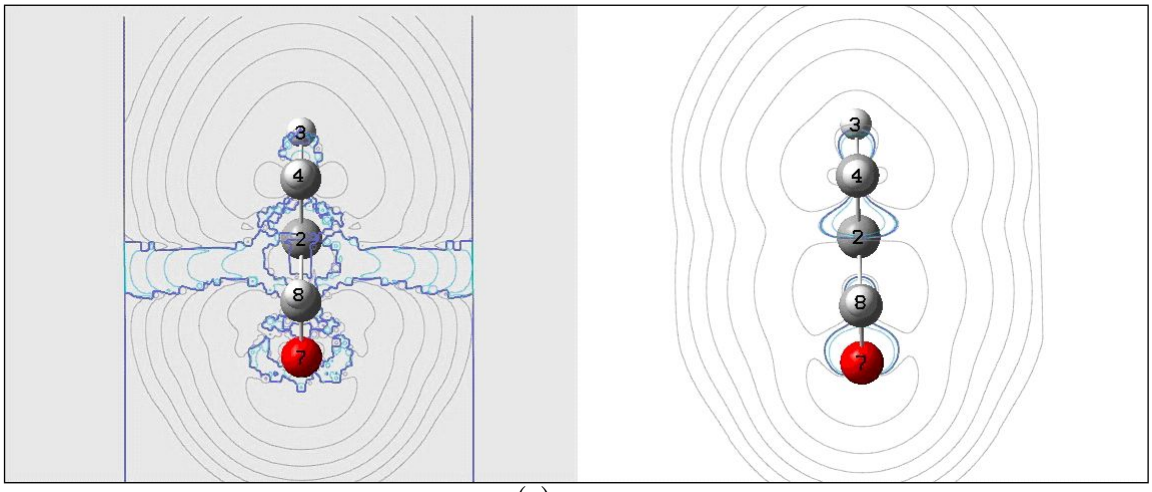

Figure S58. Left) Fukui function $f(\mathbf{r})_{\text{Quadratic expansion}}$ calculated with a parabolic approximation (Eq. 23) and right) hardness function $\eta(\mathbf{r})$ (Eq. 13) for the CH_2CHCHO molecule.

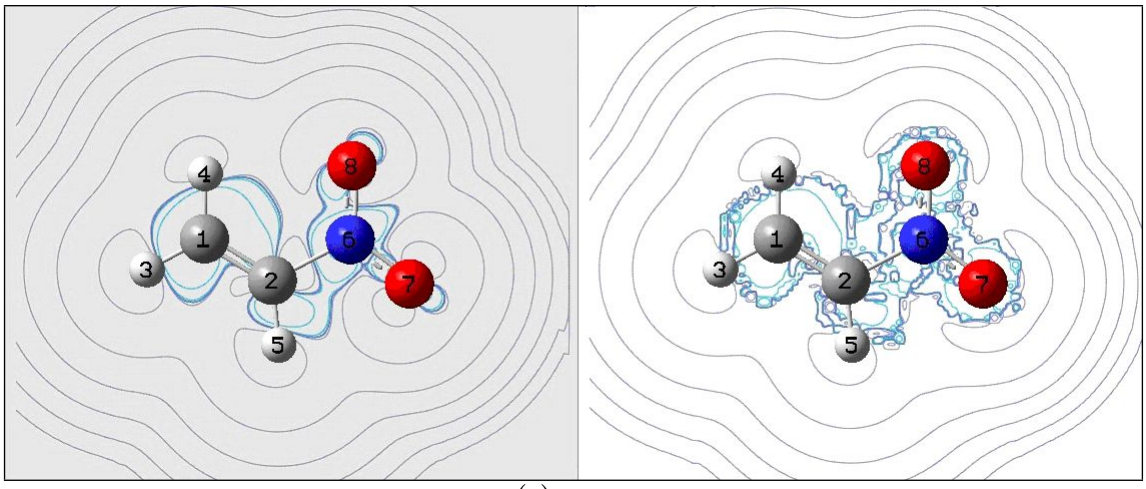

Figure S59. Left) Fukui function $f(\mathbf{r})_{\text{Quadratic expansion}}$ calculated with a parabolic approximation (Eq. 23) and right) hardness function $\eta(\mathbf{r})$ (Eq. 13) for the CH_2CHNO_2 molecule.

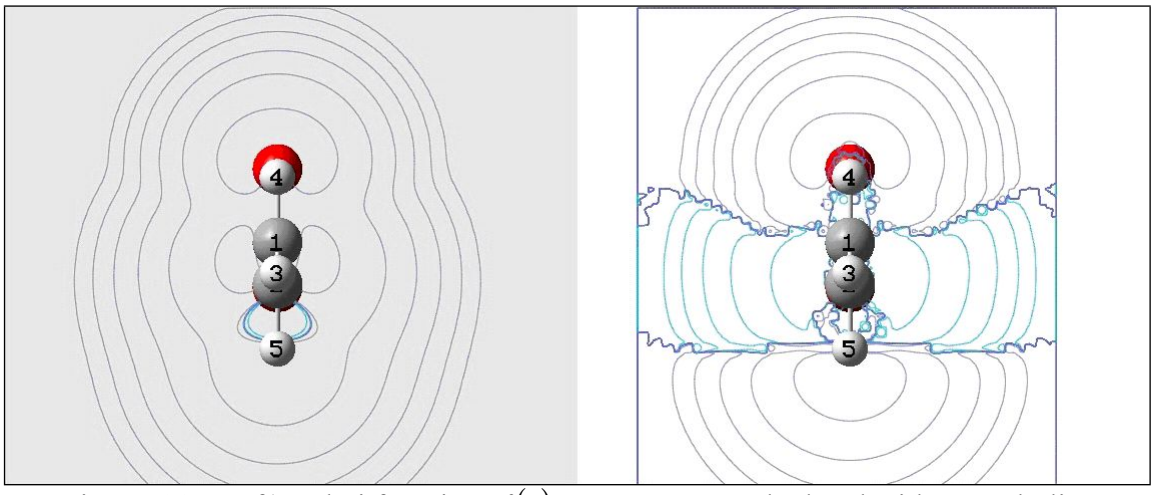

Figure S60. Left) Fukui function $f(\mathbf{r})_{\text{Quadratic expansion}}$ calculated with a parabolic approximation (Eq. 23) and right) hardness function $\eta(\mathbf{r})$ (Eq. 13) for the CH_2CHNO_2 molecule.

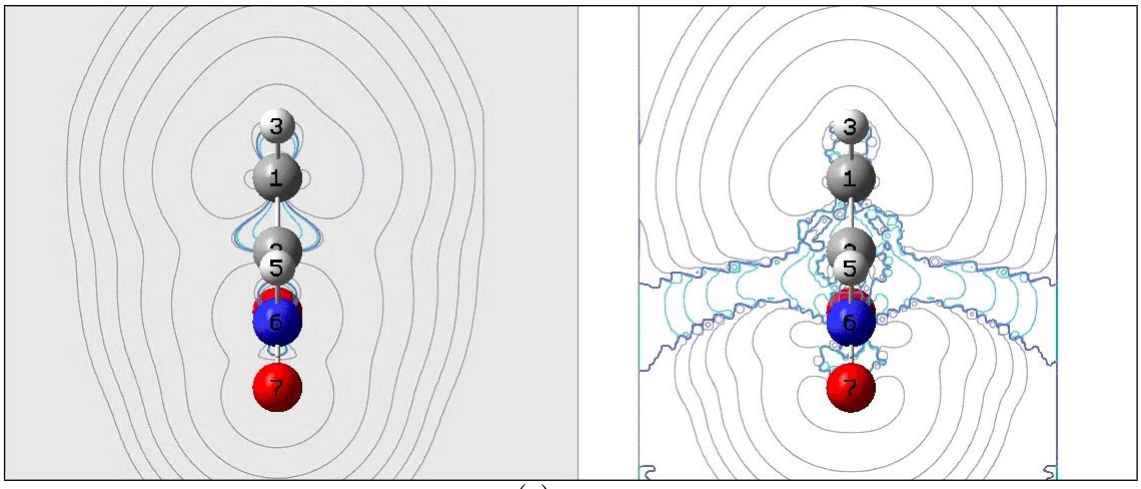

Figure S61. Left) Fukui function $f(\mathbf{r})_{\text{Quadratic expansion}}$ calculated with a parabolic approximation (Eq. 23) and right) hardness function $\eta(\mathbf{r})$ (Eq. 13) for the CH_2CHNO_2 molecule.

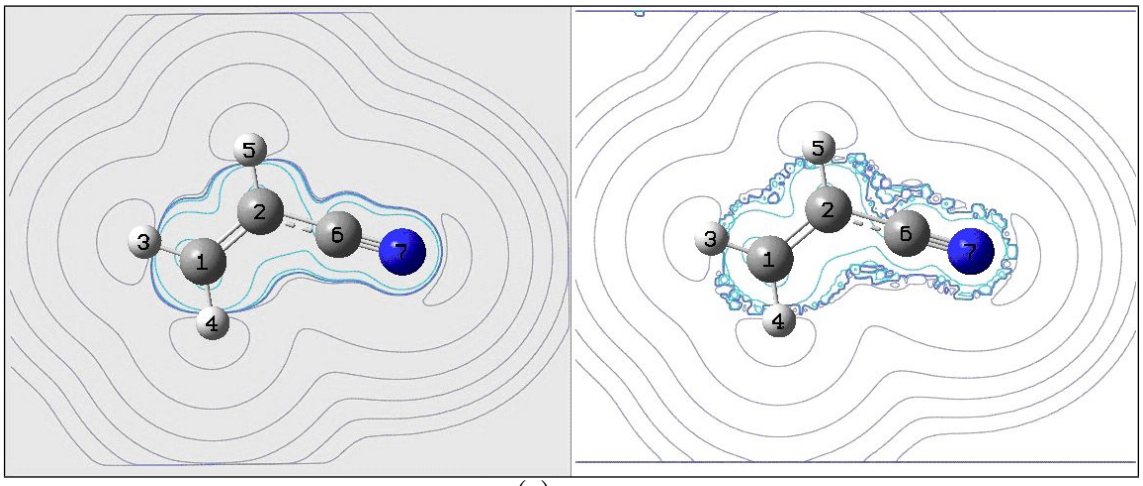

Figure S62. Left) Fukui function $f(\mathbf{r})_{\text{Quadratic expansion}}$ calculated with a parabolic approximation (Eq. 23) and right) hardness function $\eta(\mathbf{r})$ (Eq. 13) for the CH_2CHCN molecule.

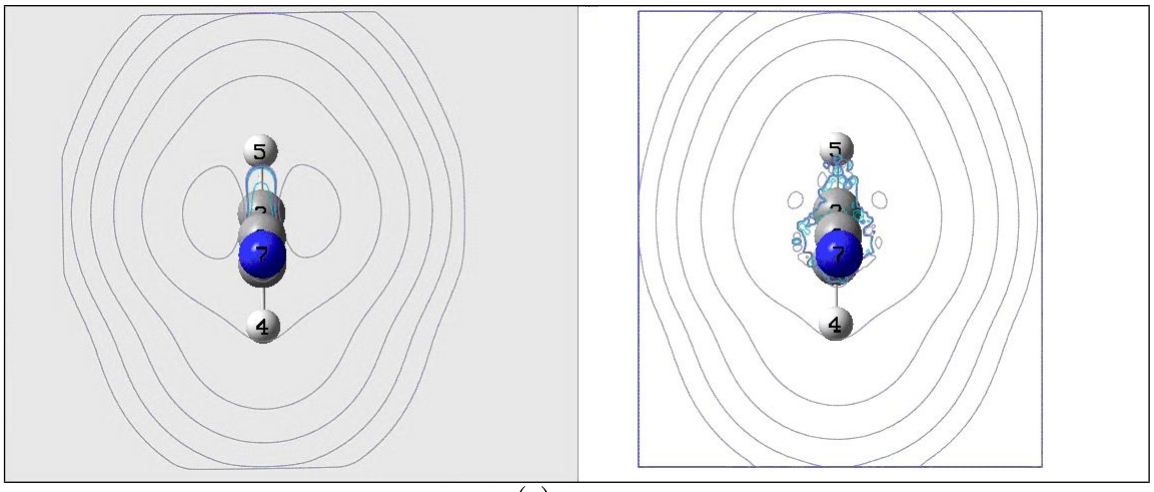

Figure S63. Left) Fukui function $f(\mathbf{r})_{\text{Quadratic expansion}}$ calculated with a parabolic approximation (Eq. 23) and right) hardness function $\eta(\mathbf{r})$ (Eq. 13) for the CH_2CHCN molecule.

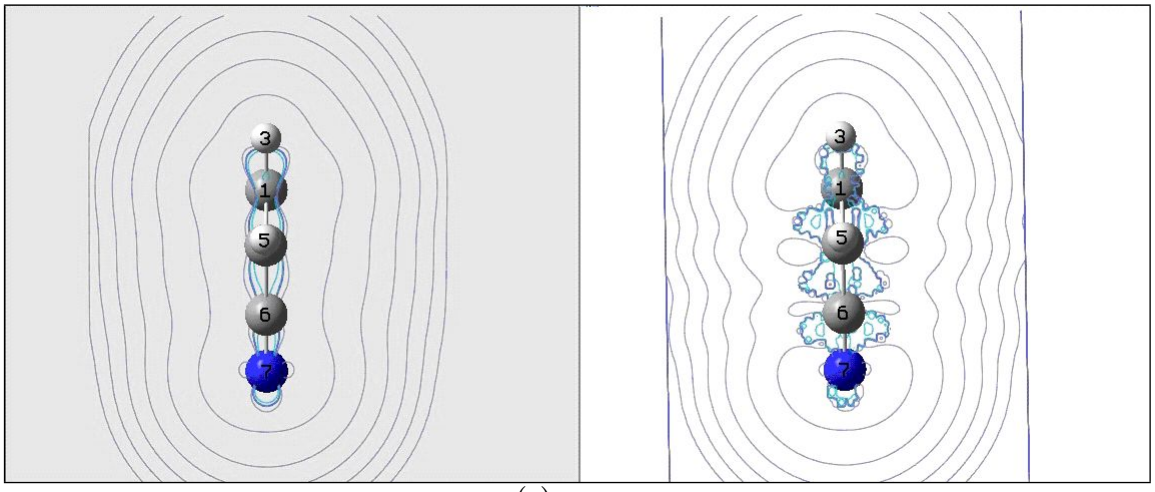

Figure S64. Left) Fukui function $f(\mathbf{r})_{\text{Quadratic expansion}}$ calculated with a parabolic approximation (Eq. 23) and right) hardness function $\eta(\mathbf{r})$ (Eq. 13) for the CH_2CHCN molecule.

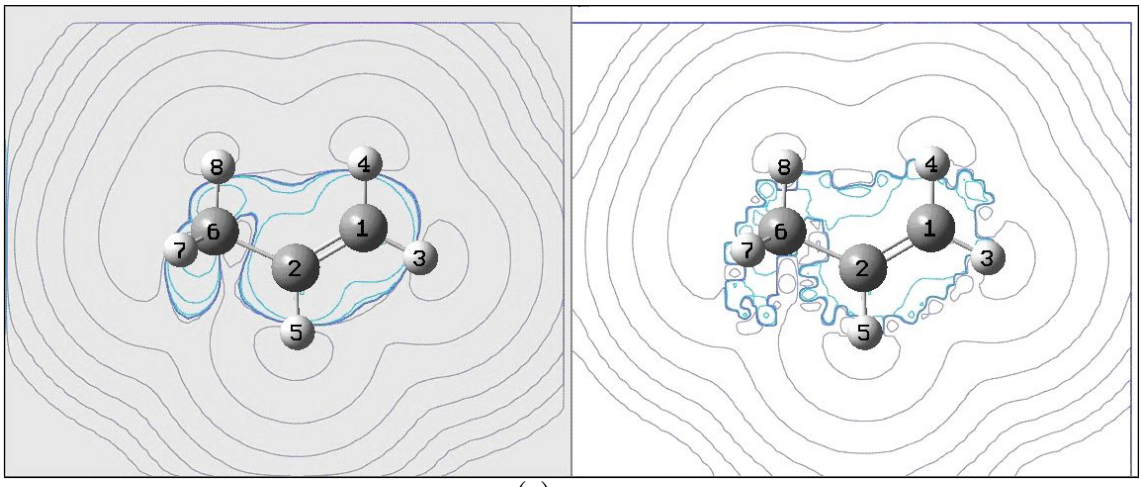

Figure S65. Left) Fukui function $f(\mathbf{r})_{\text{Quadratic expansion}}$ calculated with a parabolic approximation (Eq. 23) and right) hardness function $\eta(\mathbf{r})$ (Eq. 13) for the CH_2CHCH_3 molecule.

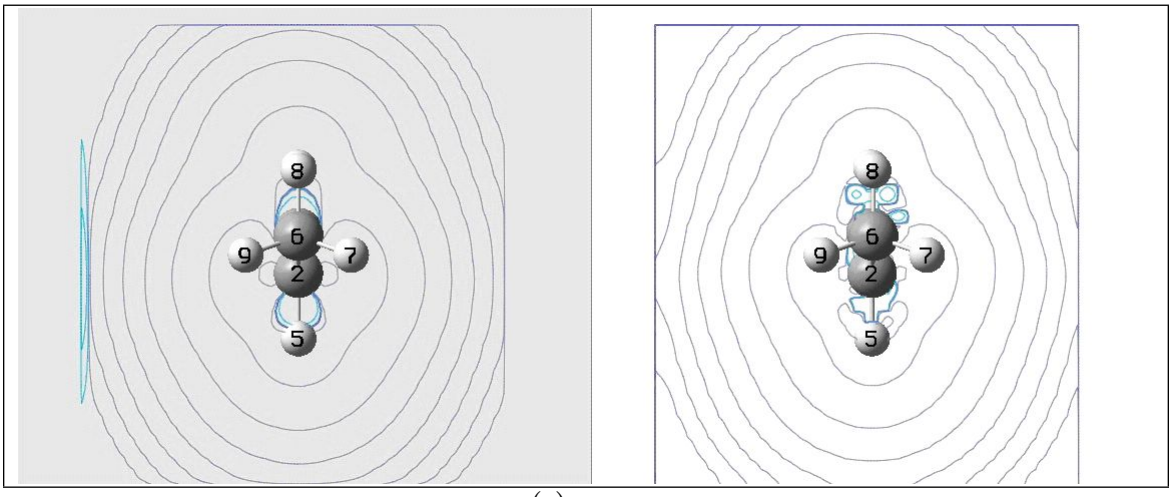

Figure S66. Left) Fukui function $f(\mathbf{r})_{\text{Quadratic expansion}}$ calculated with a parabolic approximation (Eq. 23) and right) hardness function $\eta(\mathbf{r})$ (Eq. 13) for the CH_2CHCH_3 molecule.

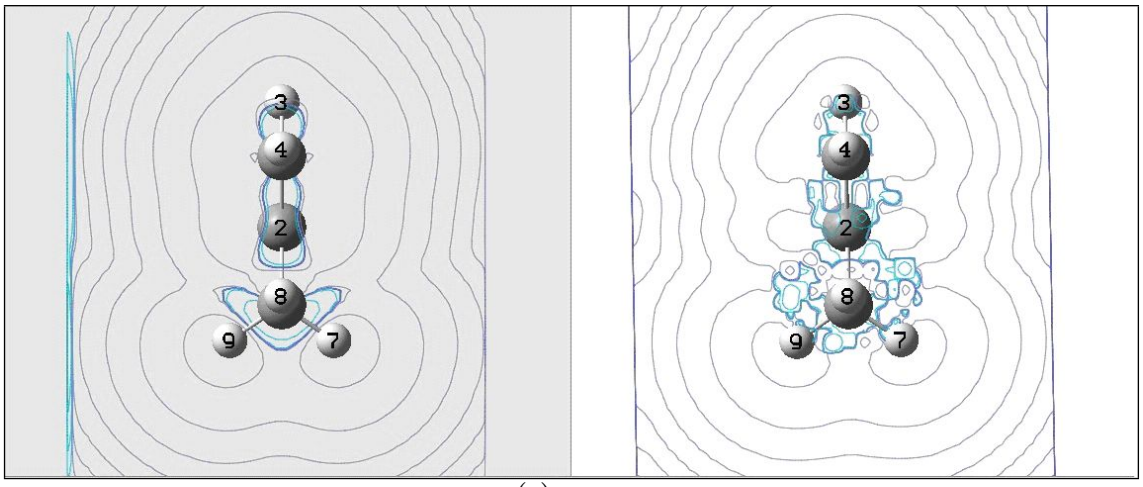

Figure S67. Left) Fukui function $f(\mathbf{r})_{\text{Quadratic expansion}}$ calculated with a parabolic approximation (Eq. 23) and right) hardness function $\eta(\mathbf{r})$ (Eq. 13) for the CH_2CHCH_3 molecule.

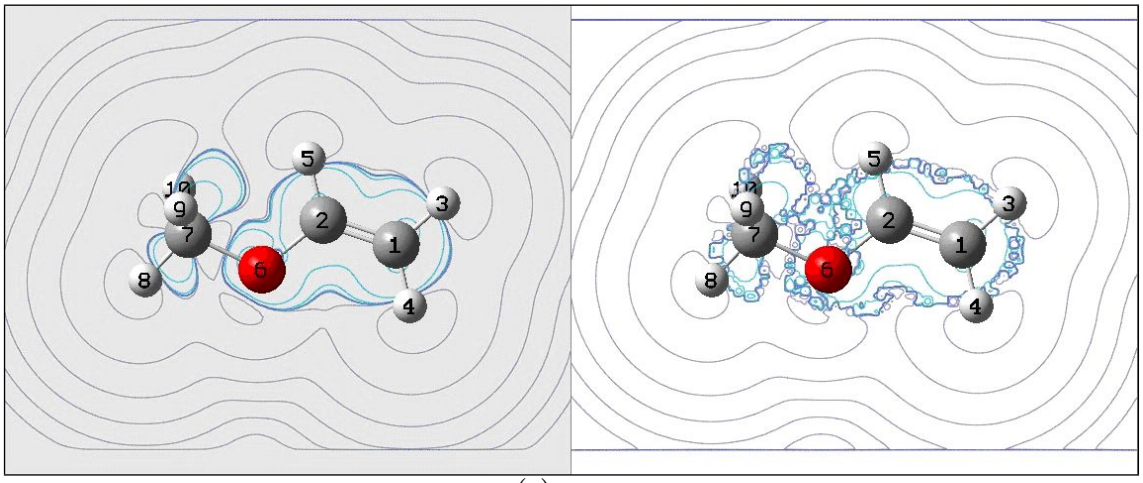

Figure S68. Left) Fukui function $f(\mathbf{r})_{\text{Quadratic expansion}}$ calculated with a parabolic approximation (Eq. 23) and right) hardness function $\eta(\mathbf{r})$ (Eq. 13) for the CH_2CHOCH_3 molecule.

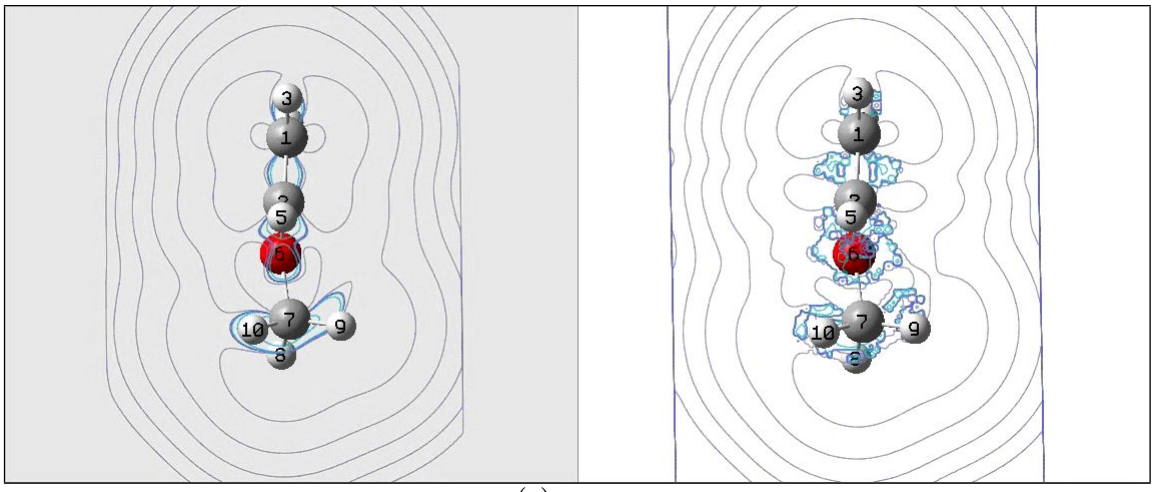

Figure S69. Left) Fukui function $f(\mathbf{r})_{\text{Quadratic expansion}}$ calculated with a parabolic approximation (Eq. 23) and right) hardness function $\eta(\mathbf{r})$ (Eq. 13) for the CH_2CHOCH_3 molecule.

APPENDIX I. Justification of some relationships between parameters of models 1 and 2.

In this appendix, some expressions used in comparisons of the main text will be justified. Starting from the model 1 and truncating from the quadratic term we obtain the expression (A1), this approximation is clearly very rough, for that reason it will only be used *to justify* the correlations studied in this work.

$$\delta E(\mathbf{r}) \approx \mu^0 \cdot \delta\rho(\mathbf{r}) + \frac{1}{2}\eta(\mathbf{r})\delta\rho^2(\mathbf{r}) \tag{A1}$$

From here we can obtain:

$$\omega(\mathbf{r}) \approx -\left(\mu^0 \cdot \delta\rho^{\max}(\mathbf{r}) + \frac{1}{2}\eta(\mathbf{r}) \cdot \left(\delta\rho^{\max}(\mathbf{r})\right)^2 \right) \tag{A2}$$

From model 2, truncating from the first term, we can obtain the expression (A3). This approach is also very crude and, as the previous one, it will only be used *to justify* the correlations studied in this work.

$$\delta\rho^{\max}(\mathbf{r}) \approx f(\mathbf{r}) \cdot \Delta N_{\max} \tag{A3}$$

Deriving (A1) we obtain:

$$\mu \approx \mu^0 + \eta(\mathbf{r}) \cdot \delta\rho(\mathbf{r}) \tag{A4}$$

And from here we get:

$$0 \approx \mu^0 + \eta(\mathbf{r}) \cdot \delta\rho^{\max}(\mathbf{r}) \tag{A5}$$

And clearing:

$$\boxed{\delta\rho^{\max}(\mathbf{r}) \approx -\frac{\mu^0}{\eta(\mathbf{r})}} \tag{A6}$$

Reordering (A2):

$$\omega(\mathbf{r}) \approx -\left(\mu^0 \cdot \delta\rho^{\max}(\mathbf{r}) + \frac{1}{2}\eta(\mathbf{r}) \cdot \left(\delta\rho^{\max}(\mathbf{r})\right) \cdot \left(\delta\rho^{\max}(\mathbf{r})\right) \right) \tag{A7}$$

Substituting two terms $\delta\rho^{\max}(\mathbf{r})$ for $f(\mathbf{r}) \cdot \Delta N_{\max}$ and a third for $-\mu^0/\eta(\mathbf{r})$ we obtain:

$$\omega(\mathbf{r}) \approx -\left(\mu^0 \cdot f(\mathbf{r}) \cdot \Delta N_{\max} + \frac{1}{2}\eta(\mathbf{r}) \cdot \left(f(\mathbf{r}) \cdot \Delta N_{\max}\right) \cdot \left(-\mu^0/\eta(\mathbf{r})\right) \right) \tag{A8}$$

and clearing:

$$\boxed{\omega(\mathbf{r}) \approx -\frac{1}{2}\mu^0 \cdot f(\mathbf{r}) \cdot \Delta N_{\max} = \omega \cdot f(\mathbf{r})} \tag{A9}$$

Now, we start from:

$$\delta\rho^{\max}(\mathbf{r})[\text{model1}] \approx \delta\rho^{\max}(\mathbf{r})[\text{model2}] \tag{A10}$$

that is a reasonable starting point. Substituting the expressions $\delta\rho^{\max}(\mathbf{r})$ previously obtained:

$$-\frac{\mu^0}{\eta(\mathbf{r})} \approx f(\mathbf{r}) \cdot \Delta N_{\max} \tag{A11}$$

Reordering:

$$-\frac{\mu^0}{\Delta N_{\max}} \frac{1}{\eta(\mathbf{r})} \approx f(\mathbf{r}) \tag{A12}$$

Finally, clearing:

$$\boxed{\eta(\mathbf{r}) \approx \frac{\eta}{f(\mathbf{r})}} \tag{A13}$$

If we start from (A2) and take into account (A6), replacing and operating we get:

$$\omega(\mathbf{r}) \approx \frac{(\mu^0)^2}{\eta(\mathbf{r})} - \frac{1}{2} \cdot \eta(\mathbf{r}) \cdot \frac{(\mu^0)^2}{\eta(\mathbf{r})^2} \tag{A14}$$

Simplifying:

$$\boxed{\omega(\mathbf{r}) \approx \frac{(\mu^0)^2}{2\eta(\mathbf{r})}} \tag{A15}$$

If we combine (A6) and (A2) and we operate we obtain:

$$\omega(\mathbf{r}) \approx -\left(\mu^0 \cdot \delta\rho^{\max}(\mathbf{r}) + \frac{1}{2}\left(-\frac{\mu^0}{\delta\rho^{\max}(\mathbf{r})} \right) \cdot \left(\delta\rho^{\max}(\mathbf{r})\right)^2 \right) \tag{A16}$$

Finally, simplifying and operating we obtain:

$$\boxed{\omega(\mathbf{r}) \approx -\frac{\mu^0}{2} \cdot \delta\rho^{\max}(\mathbf{r})} \tag{A17}$$

APPENDIX II. Summary of the nomenclature and definitions.

$f(r)$: Fukui function. It is defined as:

$$f(r)=\left(\frac{\partial\rho(r)}{\partial N}\right)_{v} \tag{A18}$$

f_k^+: atomic index: condensed-to-atom Fukui function for the "*k*" atom (nucleophilic attack)

f_k^-: atomic index: condensed-to-atom Fukui function for the "*k*" atom (electrophilic attack)

f_k^0, atomic index: condensed-to-atom Fukui function for the "*k*" atom for neutral (or radical) attack.

ω: global electrophilicity

ω_k^-: condensed Philicity to the "*k*" atom (electrophilic attack)

ω_k^+: condensed Philicity to the "*k*" atom (nucleophilic attack)

μ: global electronic chemical potential (negative of the electronegativity).

Calculated as:

$$\mu=\left(\frac{\partial E}{\partial N}\right)_{\upsilon} \tag{A19}$$

$\mu_A^0, \mu_B^0,$ μ_k^0: atomic hardness calculated for the neutral molecule.

$\mu_A^+, \mu_B^+,$ μ_k^+: atomic hardness calculated for the cation.

$\mu_A^-, \mu_B^-,$ μ_k^- : atomic hardness calculated for the anion.

η : global chemical hardness. Calculated as:

$$\eta = \left(\frac{\partial^2 E}{\partial N^2} \right)_{\upsilon} \tag{A20}$$

ΔN^+ : Global charge variation when the neutral molecule turns into a cation.

ΔN^- : Global charge variation when the neutral molecule turns into an anion.

ΔN_{max} : global maximum amount of electron charge.

$\Delta N_A^{\max}$: atomic maximum amount of electron charge for the *A* atom.

ΔE_{min} : global total energy decrease.

$\in_H$ and $\in_L$ correspond to the Kohn–Sham one-electron eigenvalues for the HOMO and the LUMO.

s(r): softness function. It is defined as:

$$s(r) = \left(\frac{\partial \rho(r)}{\partial \mu} \right)_{\nu} \tag{A21}$$

$s_k^{\alpha} \left(\alpha = +, -\, or\ 0 \right)$: condensed-to-atom softness (nucleophilic, electrophilic and attack).

Ω_A : atomic parameter which represents the coefficient of the cubic term in the cubic approximation. It is defined as:

$$\Omega_A = \left(\frac{\partial^3 \Delta E_A}{\partial N_A^3} \right)_{\Delta N=0} \quad \text{(A22)}$$